NUMERICAL STUDY OF MICRO-CHANNEL HEAT SINK WITH SLURRY OF WATER AND MEPCM PARTICLES

ABSTRACT

A three-dimensional numerical model was developed to analyze the performance of a micro-channel heat sink. Single phase, counter-flow design was evaluated compared to parallel-flow heat sink configuration. Straight and Zigzag channel geometry configuration were also compared. Finally, an enhancement with double phase fluid study was carried out. For the analysis, three-dimensional Navier-Stokes and energy equations for incompressible laminar flow, together with the temperature transforming model (TTM) as the melting/solidification model, were solved using a finite volume solver (Ansys-Fluent). Water with micro-encapsulated phase change material (MEPCM) at different concentration, and temperature-depended thermo-physical properties was used as a coolant for the double phase calculations. In this study, n-eicosane, at 10, 15 and 20% particle´s concentration, is been used as the phase change material (PCM). *The effect of the flume and channel geometry configuration at different coolant flow rates on the temperature distribution of the heat sink are investigated. P*arameters such as pressure drop within the channels and the maximum temperature value at the bottom surface were calculated. *Once the better heat sink configuration for the flow rates selected is known, the double phase properties and melting/solidifications model are applied to measure the total thermal enhancement at the different MEPCM particle concentration.*

The results showed that changes in the micro-channel flow rate decreases the peak temperature and increases the pressure drop. Counter flow configuration offers a better homogeneity in temperature, but parallel flow provides a better overall thermal-performance. Comparing straight and zig zag geometry channel configuration, zigzag channels offer a better thermal-performance at the same flow rate. However, over thermal resistance values of 3.5 x 10^{-5}, straight channels performed a better behavior cooling down the system at a lower energy cost. Finally, MEPCM particles addition results obtained showed a notable enhancement in the thermal-performance of the heat sink at all flow rates. Increasing mass concentration led to better thermal-performance, although this improvement come with an increase in pressure drop. In terms of efficiency, better thermal-performance is reached at a lower energy cost for low flow rates. Besides, the addition of MEPCM particles provides to both, fluid and solid bottom heated surface a better homogeneity in temperature along the longitudinal direction.

David Bujeda Juberias

Department of Aerospace and Mechanical Engineering

The University of Oklahoma, 2016/17

Nomenclature

Lx	Length of heat sink, x-direction (m)	Wa'	Distance between side wall of heat sink control volume and micro-channel (m)
Ly	Height of heat sink (m)	Wz	Width micro-channel control volume (m)
Lz	Length of heat sink, z-direction (m)	Lx1	Length of zigzag entrance part, x-direction (m)
Hc	Height of micro-channel (m)	Lx2	Distance between corners in zigzag micro-channel (m)
Wc	Width of micro-channel (m)	Lc	Distance intermediate straight zigzag sections (m)
Wa1	Distance between side wall of heat sink and micro-channel (m)	Lz1	Distance between zigzag interior corners of micro-channel and intermediate vertical plane (m)
Wa2	Distance between micro-channels (m)	Ac1	Angle between first zigzag section and entrance section (deg)
Hb1	Distance between upper wall of heat sink and micro-channel (m)	Ac2	Angle between zigzag sections (deg)
Hb2	Distance between bottom wall of heat sink and micro-channel (m)	v	Velocity (m/s^2)
n	Number of channels	u, v, w	Velocity components in x, y and z directions (m/s)
k	Thermal conductivity (w/m K)	t	Time (s)
μ	Dynamic viscosity (Pa s)	A	Area (m^2)
$\boldsymbol{\alpha}$	thermal diffusivity (m^2/s)	ρ	Density (kg/m^3)
q''	Heat flux (W/m^2)	h	Enthalpy (J)
h	Heat transfer coefficient (W/m^2K)	T	Temperature (K)
Δp	Pressure drop (Pa)	T_m	PCM melting temperature (K)
R_{th}	Thermal resistance (K/W)	ΔT	PCM melting temperature range (K)
P	Pumping power (W)	c_p	Heat capacity of the fluid at constant pressure (J/kg K)
$\check{T}$	Dimensionless Temperature	h_{sl}	Latent heat of fusion of PCM (J/kg)
$\check{P}$	Dimensionless pressure drop	D_H	Hydraulic diameter (m)
Nu	Nusselt number	P_w	Wet perimeter (m)

Subscripts

s	Solid	in	Inlet
l	Liquid	out	Outlet
m	Mushy zone	avg	Average value
max	Maximum value	c	Cross section
b	Base	tot	Total
ch	Channel		

INDEX

1. INTRODUCTION

The latest and fast development of electronic devices has meant microchips to get smaller till its miniaturization. The electronic packing procedures have become more sophisticated, so the electronic cooling issues increase drastically. An increase in heat production is the main problem that new cooling systems must face. The chip surface heat flux could reach values around 100 W/cm^2 and above. The malfunction rate of components increases exponentially as the system temperature increases **over the level of 80 °C. Raising the device temperature by 1°C leads to its reliability to decrease by 5%** [1].

Because of their simplicity and low cost-effective design, air-cooled heat sinks have been extensively used so far. However, the efficiency of these systems is reaching its limit, and therefore they cannot meet the cooling requirements any more. For that reason, new and more efficient cooling systems must be suggested. The idea of micro-channel heat sink was in first place introduced by *Tucker and Pease* [2] in 1981, when they used direct passage of water throughout micro-channels and carried out experiments with several micro-channels arrays. The results proved that single phase micro-channel heat sink using water as the coolant could carry away up to 790 W/cm^2 heat flux. The enhanced thermal transport properties offered by liquids have attract researchers to use them in new, condensed and more complex and refined coolant designs. Water is the most extensively used liquid due to its good thermo-physical properties.

Micro-channels have the advantage of large surface area to volume, a simple assemblage, small mass and compact size. To these characteristics, micro-chips also have a high convective heat transfer coefficient. *Qu and Mudawer* [3] studied the heat transfer characteristics of a rectangular micro-channel heat sink using water as the working cooling fluid. Their results proved that the temperature increases almost linearly along the flow direction for both, liquid and solid regions. *Afzal Husain and Kwang-Yong Kim* [4] carried on numerical analyses on the optimization of geometric parameters (channel width and gap between channels), for rectangular micro-channels under diverse boundary conditions. Two functions were utilized to optimize the micro-channel design; one was thermal resistance related to the heat transfer behavior, and the other was pumping power to push the coolant liquid throughout the channel. **The results showed that geometric parameters have a notable effect on the thermal-performance,** and between thermal resistance and pumping power.

Apart of the most conventional single layer micro-channels designs, analysis of two-layer micro-channel heat sink have also been investigated. *Kambing Vafai and Lu Zhu* [5] suggested a double layer, counter flow design. After that, *Danish Ansari and Kwang-Yong Kim* [6] worked with parallel flow and transverse-flow configurations. In these studies, it was proved a notable decrease in temperature at the bottom surface, and that the pressure drop needed for the two layered designs can be way smaller than that for one layered devices when little temperature variation is required. Also, that the transverse-flow configuration showed lower thermal resistance values compared to the parallel flow configuration.

About single layer configurations, some interesting studies were accomplished by *Fengli Zhang, Bengt Sunden, Weihong Zhang, and Gongnan Xie* [7], where parallel and counter flow configurations with bifurcations designs were compared with each other. The results showed some important

conclusions. **The thermal-performance of parallel flow micro-channel heat sink is better than the equivalent counter flow configuration**. The thermal resistance decreases with the increase of inlet velocity; however, we cannot carelessly increase the flow rate to improve the heat transfer performance. Also, with regard to the bifurcated channel designs, they exhibited a better performance but with an increase in pressure drop.

All the studies mentioned so far were carried out with single phase cooling liquids, like water. However, the improve in the state of the art allow us to improve the designs constantly, every year; and what is more, as new materials are discovered, more refined configurations can be employed. A phase change material (PCM) is a material with a high latent heat of fusion, which on melting and solidification, is able to absorb and release large amounts of heat. The large latent heat of PCM particles is linked with its high effective thermal conductivity, accomplishing high heat fluxes with small temperature deviations. Previous studies suggested that combining micro-encapsulated phase change material (MEPCM) particles can enhance the heat transfer significantly [8-10]. *R. Sabbah, Mohammad M.Farid, S. Al-Hallaj* [8] carried out a numerical study with water and MEPCM particles as a double phase liquid coolant. They stated that using MEPCM slurries is more efficient than just increasing the flow rate; however, to get remarkable enhancement for a certain heat flux, the cooling system ought to be designed so that the MEPCM particles start melting at the channel inlet and they should be completely melted by the time the particles reach the channel exit. *S. Kuravi, Krishna M. Kota, J. Du and Louis C. Chow* [9] numerically checked parameters such as melting range of the PCM and heat flux, inlet temperature and particle concentration. They stated that the presence of MEPCM particles inside the fluid leads to the increment of the Nusselt number and decreases the slurry mean temperature. An increase in mass concentrations of the PCM helps in the improvement of heat transfer. At the same time, of course, due to the increase in the effective viscosity of the fluid, the pressure drop inside the channel rises in the case of the slurry. *B. Rajabifar, Hamid R. Seyf, Y. Zhang, Sanjeev K. Khanna* [10] performed another numerical study, but this time they put in practice a different design with micro pin fin heat sink. They proved that the MEPCM slurry has a drastic effect on the Euler number, and with incrementing the volume fraction and decreasing the inlet velocity, the Euler number increases in consequence.

Apart of numerical studies, several experimental analyses have been performed and serve us for validating the numerical data accesible for the PCM slurries. Goel et al. [11] experimentally tested PCM slurries under forced laminar flow conditions with constant heat flux. They announced a reduction in the wall temperature by up to 50% when using PCM slurry compared with water for the same dimensionless parameters. The wall temperature was also decreased by increasing the microcapsule diameter from 100 μm to 250 μm. Inaba [12] experimentally examined the performance of PCM slurries in both, laminar and turbulent flow regions with a constant heat flux. The viscosity and thermal conductivity of the slurries were also measured. The conclusions revealed agreement between the measured values, Maxwell's correlation for thermal conductivity and Vand's correlation for viscosity.

Regarding the numerical approximations employed by many to simulate the phase change process when the MEPCM particles melt, in the last 20 years a lot of numerical techniques have been developed. These techniques can be divided into two main groups (Voller, 1997): fixed grid schemes, or weak numerical solutions, and deforming grid schemes, or strong numerical solutions. Fixed grid

schemes have a simpler mathematical structure than deforming grid scheme, and fairly accurate results can be achieved (Cao and Faghri, 1990). There are three main methods in the group of fixed grid schemes: **equivalent heat capacity method, enthalpy method and temperature transforming model** [15]. The enthalpy method can deal with both mushy and isothermal phase-change problems but the temperature at a typical grid point may oscillate with time. The equivalent heat capacity model generates results without oscillations but has difficulty handling cases where the phase-change temperature range is small. The **temperature transforming model** (TTM), means an improved heat capacity method, in which the enthalpy-based energy equation is converted into a nonlinear equation with a single dependent variable (temperature). The simulations of the TTM method shown by Cao and Faghri (1990) are precise enough compared with experimental results and it also offers a simple structure and an efficient computational time.

Although some studies on improving the performance of micro-channels have been carried out, still exist some issues that could be enhanced. As it's been shown, different kinds of flumes configurations have been treated and researches have been working with the idea of PCM slurries to increase the heat transfer. However, the **temperature distribution at the bottom surface**, the one in contact with the heat source, in all these studies it's not **homogenous**. What it means that there will be unwanted hot spots at that surface. Besides, not many studies in **channel configuration** have been reported for multiphase liquids as the cooling working fluid. And the ones that tried to deal with the micro-channel design use a simple approximation for modelling the specific heat capacity. This parameter reaches significance importance when the PCM particles are melting, so the way in which this process is defined will mean getting valid or wrong results. According to this parameter **better approaches for modeling the specific heat capacity** could be used. On this study, going a step further, the **Temperature Transforming Model** (TTM) will be implemented.

In this study, the focus is on **single layer**, **counter and parallel flow configuration**, where water and a slurry, water with MEPCM particles, have been used as the coolant liquids to enhance the overall thermal-performance. Two different **channel geometry configurations** are proposed, **straight and zigzag** channel configuration. A three-dimensional numerical model is developed to analyze the corresponding laminar flow and thermal-performance of the micro-channel heat sink. A constant uniform heat flux condition is applied at the bottom wall, where the heat generating chips will be located**. The main objective of this study is to obtain an understanding of the effects of flow and channel configuration for micro-channel heat sinks with MEPCM slurries as the multi-phase coolant liquid, where a better modelling approximation will be used for the melting/solidification process.** The thermal-performance s in terms of pressure drop and temperature distribution as a function of the total flow rate, along the heat sink micro-channels, are provided and analyzed. Besides, heat sink performances at low flow rates will be preferred, so an optimal point between total pumping power required by the system and thermal-performance enhancement is reached.

2. PHYSICAL MODEL

A schematic diagram of the proposed single layered micro-channel heat sink designed is shown in Fig. 1. The complete heat sink body is composed of one layer of micro-channels with **33 channels** in total. The design is arranged in such a way that, apart from the regular parallel flow configuration, the direction of the fluid flow can be alternated to stablish a counter flow between each pair of channels. Per the periodic condition, to reduce the total number of grid elements, and so the computational time, just two micro-channels were taken as the computational model.

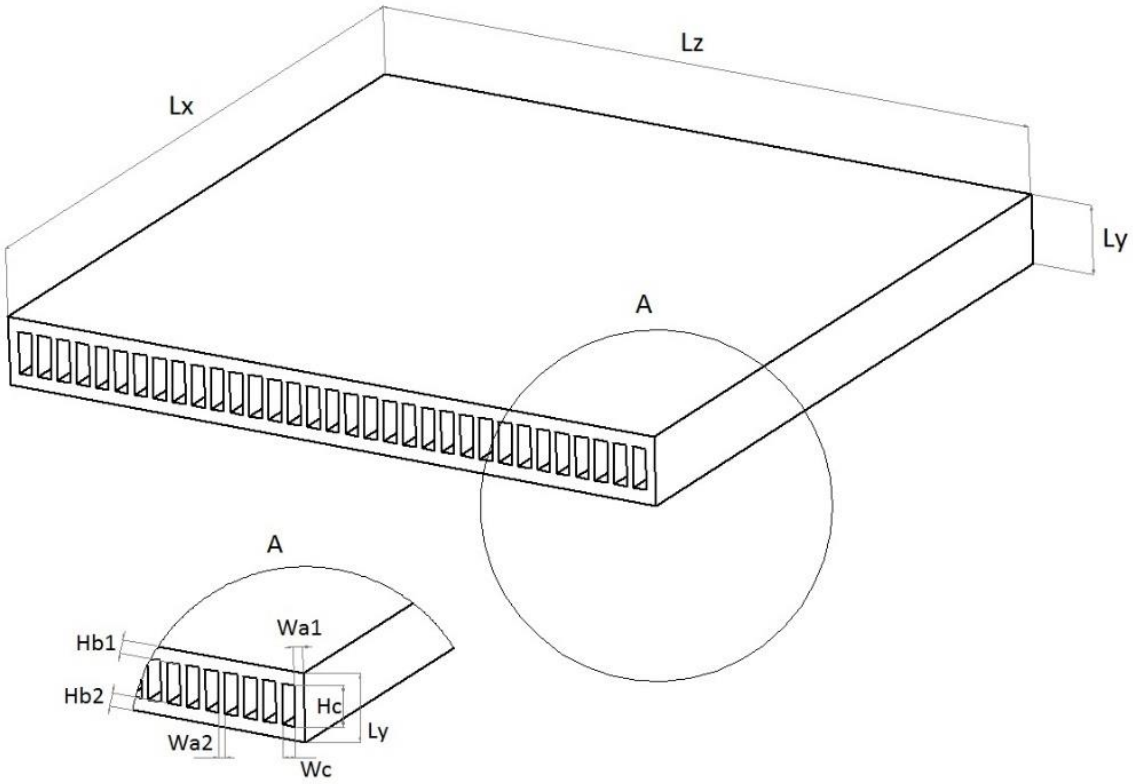

Figure 1 – Heat Sink geometry

For this study, two channel configurations were considered, straight and zigzag. Both control volumes are shown in Fig.2 and Fig.3, respectively. The geometric parameters of the micro-channel heat sink are listed in Table 1 and 2.

For the zig zag configuration, different channel structures were proposed. Eventually, the design chosen is composed by an initial and final part (1); and the central part (2), where the same zigzag structure is repeated 9 times.

Regarding these two-channel geometry configuration, a total of 4 cases were tested. Counter and parallel flow for both, straight and zigzag channel configuration.

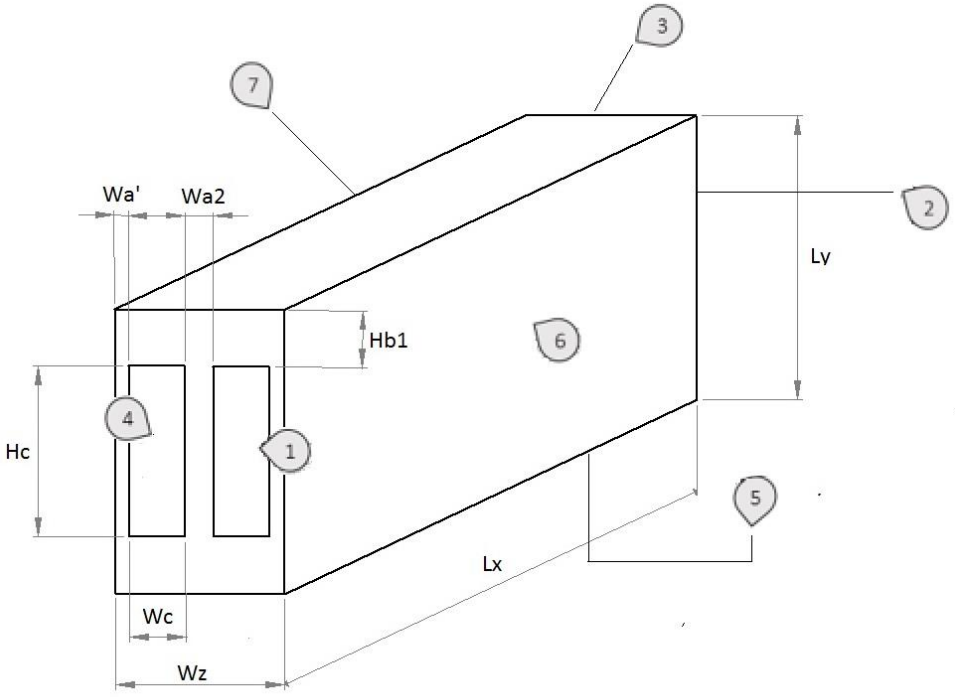

Figure 2 – Straight channel configuration control Volume

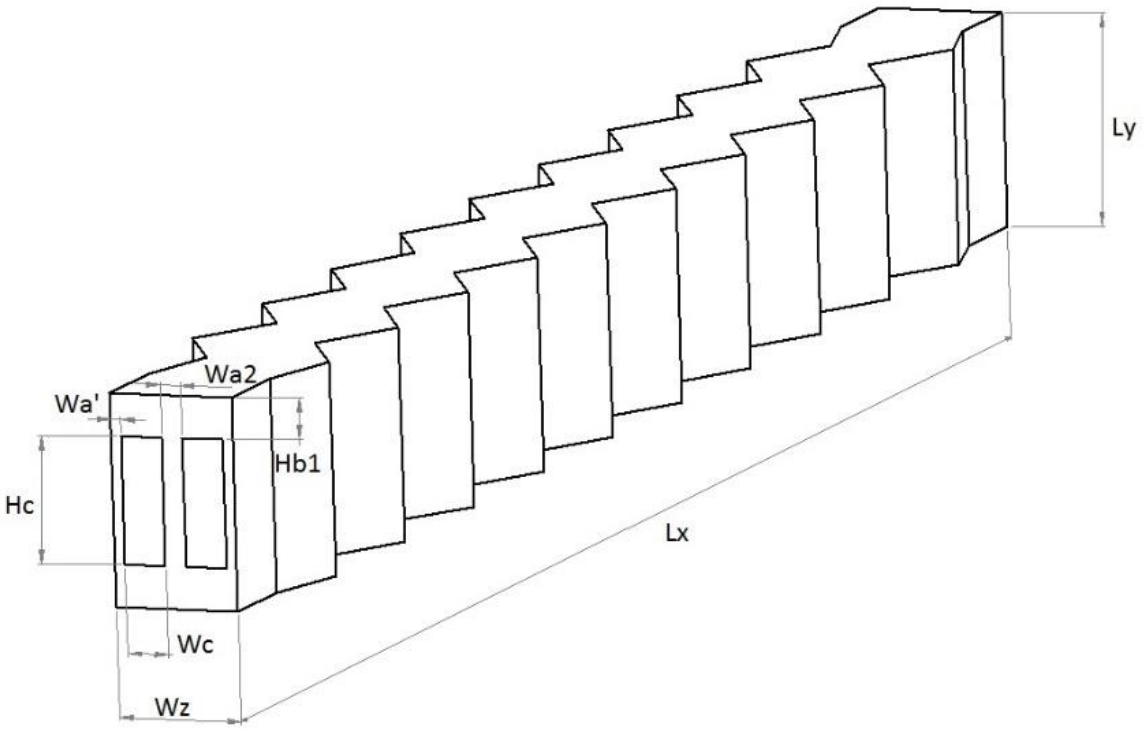

Figure 3 - Zigzag channel configuration control Volume

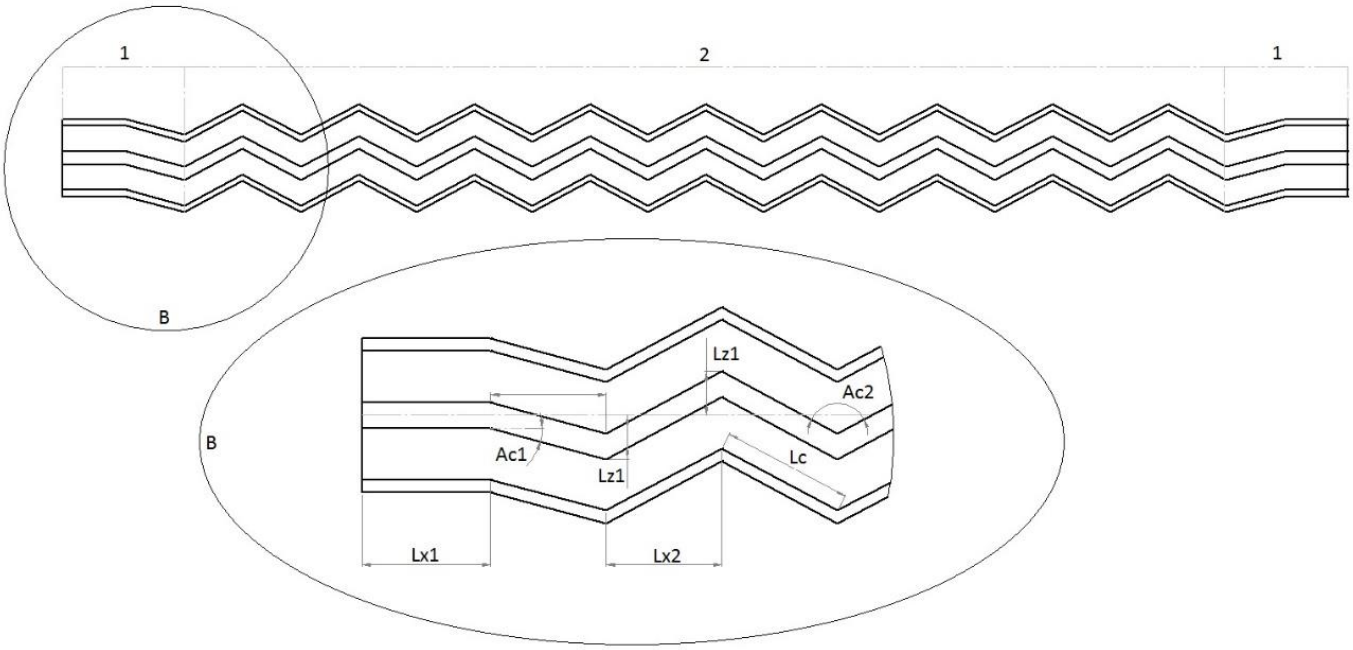

Figure 4 – Zigzag channel configuration control Volume detailed view

Table 1 – Micro-Channel heat sink dimensions (mm)

Lx	Lz	Ly	Hc	Wc	Wa1	Wa2	Hb1	Hb2	Wa’	Wz
10	10	1	0.6	0.2	0.15	0.1	0.2	0.2	0.05	0.6

Table 2 - Micro-channel zigzag specific dimensions (mm)

Lx1	Lx2	Lc	Lz1	Ac1(deg)	Ac2(deg)
0.5	0.45	0.51	0.17	15	123.63

3. SOLUTION METHODOLOGY

3.1. GOVERNING EQUATIONS

Three-dimensional numerical calculations were carried out for fluid and heat transfer performance in micro-channel heat sinks using commercial computational fluid dynamic code, ANSYS-fluent CFD. A multigrid solver it's been used for solving the governing equations for **mass**, **momentum**, and **energy**. An element-based finite volume approximation was used for solving these equations. Mass, momentum and energy were solved until the root-mean-square residuals were less than 10^{-6}, when the convergence was considered accomplished. The coupling of pressure and velocity fields was handle by the Semi-Implicit Method for Pressure Linked Equations (SIMPLE) algorithm.

Calculations for both, single and double phase have been carried out in this study. The characteristics for these two cases are described below.

3.1.1. Single phase fluid

To study the flow and heat transfer characteristics of the three-dimensional models under the assumption of single phase cooling liquid, several assumptions are made as follow:

- The influence of gravity it's been neglected;
- The flow is a single phase, laminar and in steady state;
- The thermal physical properties of the fluid and solid do not vary with temperature.

The procedure to calculate the different cases using just water as the cooling liquid has been very straight forward. The fluid properties and thermal behavior considered to calculate the thermal-performance of the heat sink designs have been given by the software.

3.1.2. Double phase fluid

Similar procedure it´s been followed when solving with the software for double phase fluid calculations. However, different liquid thermo-physical properties have been used. In the case of the double phase fluid (water + MEPCM particles), th**e fluid still it´s been considered as single phase** when solving with FLUENT. The meting/solidification model and the effective properties of the slurry have been calculated and given to the solver, modifying the thermal and physical properties of the working fluid (slurry). Besides, the multi-phase model is based on the next assumptions:

- The influence of gravity it's been neglected;
- The flow is a single phase, laminar and in a transient state;
- The total melting range of MEPCM particles is 2 degree;
- The particle distribution is homogeneous so that the bulk properties are assumed constant; except for thermal conductivity and heat capacity, which are functions of temperature;
- The particle melts instantaneously, there is no temperature gradient inside the particle [23];
- The MEPCM-slurry enthalpy consists of two parts: sensible heat and PCM latent heat.

Apart of these assumptions, due to the transient nature of the calculations, and because of the added melting model hocked to FLUENT, the time step and the under-relaxation factor for the energy equation took relevance importance. So, in order to achieve full convergence and valid results, the under-relaxation factor for the energy equation was stablished in 0.9. For the time-step, as long as the error in the residuals is kept under a minimum during the first iterations, not further troubles should be found when increasing this value to speed up the calculation process.

3.1.2.a. Melting/Solidification model

When solving the melting/solidification problem, the approximation used in the references given on this study it´s been the Equivalent Heat Capacity model. Another method is the Temperature Transforming model, which combines the advantages of the enthalpy and equivalent heat capacity models [15]. For a three-dimensional phase change problem, the energy governing equation in enthalpy form is:

$$\frac{\partial \rho h}{\partial t} + \frac{\partial \rho u h}{\partial x} + \frac{\partial \rho v h}{\partial y} + \frac{\partial \rho w h}{\partial z} = \frac{\partial}{\partial x}\left(k\frac{\partial T}{\partial x}\right) + \frac{\partial}{\partial y}\left(k\frac{\partial T}{\partial y}\right) + \frac{\partial}{\partial z}\left(k\frac{\partial T}{\partial z}\right) \tag{1}$$

For a phase change occurring over a temperature range ($T_m - \Delta T, T_m + \Delta T$) with the specific heats considered to be constant for each phase, the relationship between enthalpy and temperature can be plotted as in Fig.5. This relationship can be analytically expressed as:

$$h(t) = \begin{cases} c_{ps}(T - T_m) + c_{ps}\Delta T & T < T_m - \Delta T \\ \left(\frac{c_{ps} + c_{pl}}{2} + \frac{h_{sl}}{2\Delta T}\right)(T - T_m) + \frac{c_{ps} + c_{pl}}{2}\Delta T + \frac{h_{sl}}{2} & T_m - \Delta T < T < T_m + \Delta T \\ c_{pl}(T - T_m) + c_{ps}\Delta T + h_{sl} & T > T_m + \Delta T \end{cases} \tag{2}$$

By defining specific heat in the mushy zone as:

$$c_m = \frac{c_{ps} + c_{pl}}{2} \tag{3}$$

Equation 2 becomes

$$h(t) = \begin{cases} c_{ps}(T - T_m) + c_{ps}\Delta T & T < T_m - \Delta T \\ \left(c_m + \frac{h_{sl}}{2\Delta T}\right)(T - T_m) + c_m\Delta T + \frac{h_{sl}}{2} & T_m - \Delta T < T < T_m + \Delta T \\ c_{pl}(T - T_m) + c_{ps}\Delta T + h_{sl} & T > T_m + \Delta T \end{cases} \tag{4}$$

Equation 4 can be rewritten as

$$h(t) = c_p(T)(T - T_m) + b(T) \tag{5}$$

Where T_m correspond to the melting point.

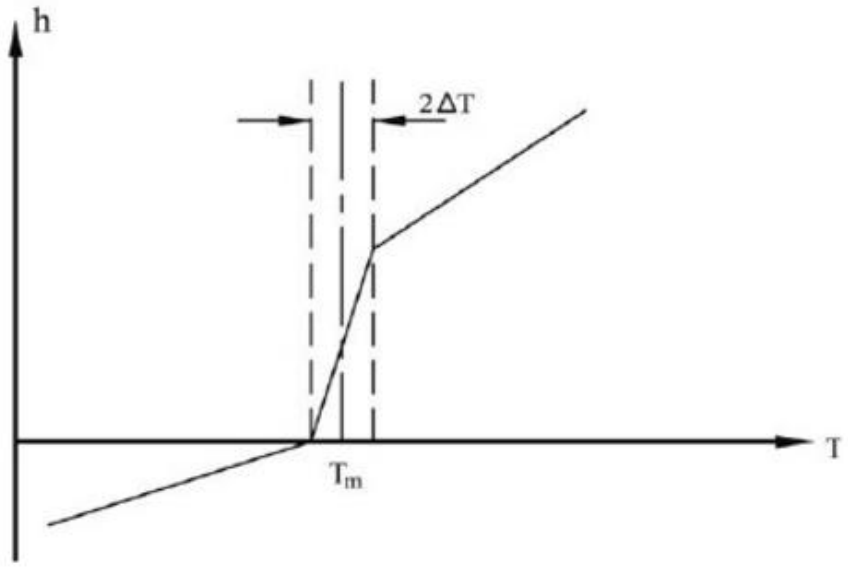

Figure 5 - Dependence of enthalpy on temperature for phase change occurring over a temperature range ΔT

Where $c_p(T)$ and $b(T)$ can be determined from equation 4.

$$c_p(T) = \begin{cases} c_{ps} & T < T_m - \Delta T \\ \left(c_m + \frac{h_{sl}}{2\Delta T}\right) & T_m - \Delta T < T < T_m + \Delta T \\ c_{pl} & T > T_m + \Delta T \end{cases} \tag{6}$$

$$b(T) = \begin{cases} c_{ps}\Delta T & T < T_m - \Delta T \\ \left(c_m \Delta T + \frac{h_{sl}}{2}\right) & T_m - \Delta T < T < T_m + \Delta T \\ c_{ps}\Delta T + h_{sl} & T > T_m + \Delta T \end{cases} \tag{7}$$

Substituting equation 5 into equation 1 yields:

$$\frac{\partial \rho c_p T^*}{\partial t} + \frac{\partial \rho u c_p T^*}{\partial x} + \frac{\partial \rho v c_p T^*}{\partial y} + \frac{\partial \rho w c_p T^*}{\partial z} = \frac{\partial}{\partial x}\left(k\frac{\partial T}{\partial x}\right) + \frac{\partial}{\partial y}\left(k\frac{\partial T}{\partial y}\right) + \frac{\partial}{\partial z}\left(k\frac{\partial T}{\partial z}\right) - \left(\frac{\partial \rho b}{\partial t} + \frac{\partial \rho u b}{\partial x} + \frac{\partial \rho v b}{\partial y} + \frac{\partial \rho w b}{\partial z}\right) \tag{8}$$

where $T^* = T - T_m$. The thermal conductivity, k, is a function of temperature and can be obtained by equation 9.

$$k(T) = \begin{cases} k_s & T < T_m - \Delta T \\ k_s + \dfrac{k_l - k_s}{2\Delta T}(T - T_m + \Delta T) & T_m - \Delta T < T < T_m + \Delta T \\ k_l & T > T_m + \Delta T \end{cases} \quad (9)$$

The energy equation has been transformed into a nonlinear equation, equation 8, with just a single dependent variable, Temperature (T). **The last terms within the brackets correspond to the additional source term** that one must include when solving to overcome the equivalent Heat Capacity model restrictions, and get more accurate results.

The temperature transforming model eases the time-step and grid-size selection and is also insensitive to the phase change temperature range.

So, the energy equation will be resolved, but with an additional source term and with temperature dependent functions for the heat capacity and thermal conductivity. The way to implement these additional equations in the solver will be using macros given by ANSYS in the form of UDF (User Defined Functions) [16].

3.1.2.b. Thermal properties of the slurry

On this case, the working fluid or slurry is going to be a combination of water and encapsulated phase change material particles. Both, physical and thermal properties at different PCM particle concentrations are going to change. Different approximations to obtain the valid working values have been used in other studies.

In a previous study [17], microcapsules of n-eicosane ($C_{20}H_{42}$) in an amino formaldehyde resinous all were tested for use in microencapsulated phase change suspensions. Since these microcapsules were found to be structurally and thermally stable, they were used in the present study. The properties of the phase change material and the wall of the microcapsules are given in Table 3.

Table 3 – PCM, capsule material & Water properties

Material	density (kg/m^3)	Thermal conductivity (W/mK)	Dynamic viscosity (Pa s) - μ	Specific heat capacity (j/kg K) - cp	hsl (J/kg)
water	998.2	0.6069	0.000899	4180	-
n-eicosane (solid)	856	0.15	-	1920	247300
n-eicosane (liquid)	778	0.15	-	2460	
Urea-formaldehyde Microcapsulated	1500	0.42		1672	-

Water was chosen as the working fluid because its properties and because is easy to handle and has no effects on the phase change material or the microcapsule wall. In addition, the density of the microcapsules is close to the water density, so that a nearly homogeneous mixture could be obtained.

- Microcapsule properties

The PCM, n-eicosane, made up about the 70% of a microcapsule by weight [17]. This percentage was taken as an approximation to define the portion of core and wall forming the MEPCM. The 70% in diameter correspond to the core, and the 30% respect to the total particle diameter is composed by the wall. The thermos-physical properties of n-eicosane and the wall material are different, so the properties of the microcapsules should be obtained by considering the properties of each of the components. The density of the microcapsules was calculated using a simple weighted average approximation. The specific heat of the microcapsules was calculated using energy balance. The density and specific heat of n-eicosane was taken as the mean of its solid and liquid densities [18].

$$\rho_p = \left(\frac{d_c}{d_p}\right)\rho_e + \left(\frac{d_w}{d_p}\right)\rho_w \tag{10}$$

$$c_p = \frac{(7c_e + 3c_w)\,\rho_e\rho_w}{(3\rho_e + 7\rho_w)\rho_p} \tag{11}$$

Table 4 -Specific nomenclature for MEPCM and slurry properties definition

ρ_p	MEPCM density
ρ_e	Pure n-eicosane density
ρ_w	MEPCM wall density
ρ_{wt}	Water density
ρ_s	Slurry density
d_c	MEPCM core diameter
d_p	MEPCM particle diameter
c_e	Pure n-eicosane specific heat
c_w	MEPCM wall specific heat
c_s	Slurry specific heat
c_{wt}	Water specific heat
k_p	MEPCM thermal conductivity
k_e	Pure n-eicosane thermal conductivity
k_w	MEPCM wall thermal conductivity
c	MEPCM concentration

The thermal conductivity of the MEPCM was calculated using the composite sphere approach. The thickness of the microcapsule wall determined the heat transfer resistance of the wall, while the heat transfer resistance of the core was evaluated taking into consideration the model for a solid sphere in an infinite medium [19]. The thermal conductivity of the MEPCM particles is given by:

$$\frac{1}{k_p d_p} = \frac{1}{k_e d_c} + \frac{d_p - d_c}{k_w d_p d_c}$$

(12)

- Slurry properties

The bulk slurry properties are a combination of the properties of the main cooling fluid and the microcapsules added to it. Using a mass and energy balance [18], the density and specific heat are:

$$c_s = \frac{c\rho_p c_p + (1-c)\rho_{wt} c_{wt}}{\rho_s}$$

(13)

Where the density of the slurry is given by:

$$\rho_s = c\rho_p + (1-c)\,\rho_{wt}$$

(14)

To calculate the viscosity of the slurry, the following relation by Vand [20] was used:

$$\frac{\mu_s}{\mu_{wt}} = (1 - c - 1.16c^2)^{-2.5}$$

(15)

This relation has been shown to be valid for concentrations up to 20% and duct-to-particle diameter rations of 20 - 100 and mean particle diameters of 0.3 - 400 μm.

Maxwell`s [21] relation for the bulk thermal conductivity was employed to obtain the slurry conductivity. Yamada and Takahashi [22] found good agreement between this relation and their thermal values for MEPCM particles addition at concentrations up to 22%.

$$\frac{k_s}{k_{wt}} = \frac{2 + \frac{k_p}{k_{wt}} + 2c\left(\frac{k_p}{k_{wt}} - 1\right)}{2 + \frac{k_p}{k_{wt}} - c\left(\frac{k_p}{k_{wt}} - 1\right)}$$

(16)

Finally, the values for the slurry equivalent latent heat was obtained as the weighted average value, multiplying the latent heat of pure n-eicosane by its concentration in the slurry. Assuming a fixed mean particle diameter of 200 μm, the thermos-physical for the slurry at different MEPCM particle concentration is shown in Table 5.

Table 5 - MEPCM particle and Slurry properties at different MEPCM particle concentrations

Material	density (kg/m^3)	Thermal conductivity (W/mK)	Dynamic viscosity (Pa s) - μ	Specific heat capacity (j/kg K) - cp	hsl (J/kg)
MEPCM	946.4	0.15	-	1973.1	-
Slurry 5% concentration	983	0.576	0.00102232	4098	12365
Slurry 10% concentration	975	0.547	0.001209	4014	24730
Slurry 15% concentration	966	0.519	0.0014587	3930	37095
Slurry 20% concentration	957	0.492	0.0018183	3844	49460

Where the above thermal-properties are taken as constant for all calculations. These values represent the mean value properties of their solid and liquid phases. Therefore, **same values for the liquid and solid regions apply to the temperature transforming model.**

3.2. BOUNDARY CONDITIONS

Referring to figure 2 from the physical model, the next control regions are defined:

Table 6 - Control regions for boundary conditions

	Region name	Boundary condition
1	Inlet 1	Velocity inlet
2	Outlet 1	Pressure outlet
3	Inlet 2	Velocity inlet
4	Outlet 2	Pressure outlet
5	Bottom heated surface	Wall
6	Periodic 1	Interface
7	Periodic 2	Interface

Where a parallel or counter flow conditions applies every 2 channels. For that purpose, the regions ''inlet 2'' and ''outlet 2'' can be switched between ''velocity inlet'' and ''pressure outlet''. A uniform heat flux of **100 W/cm^2** was applied to the base of the heat sink (region 5). A periodic boundary condition was set at the lateral outer boundaries surfaces of the control volume (regions 6 and 7), and all the remaining outer surfaces were kept adiabatic. A uniform velocity was assigned at the inlets of the channels, and atmospheric pressure was assigned at the outlets. All contact area between solid and fluid volume was defined as coupled wall conditions. The heat sink was assumed to be composed of **aluminum** with a thermal conductivity of 202.4 W/m K. The initial temperature conditions within the solid and the fluid domains were 300 K. W**ater** was selected as the liquid coolant for the first part of this study. **MEPCM particles** will be add to the water to get the double phase liquid approximation for the last part.

In the case of the zigzag channel control volume, the boundary conditions and the regions defined are the same.

4. RESULTS

Numerical investigations for laminar flow and thermal-performance have been carried out at different values of flow rate. The goal of this project was not only to analyze the thermal-performance enhancement due to MEPCM particles addition to a carrier fluid like water, or investigate the computational improvement that the temperature transforming model can provide. Specifically, and in the first place, based on current studies of heat sinks performed by different authors, the aim of this project is also to **verify the enhancement in homogeneity over the bottom surface**, along with the overall **thermal-performance and pumping power required** by the different heat sink configurations proposed.

Therefore, before proceeding with the double phase calculations it was necessary to analyze and fully understand the cooling capacities of the four heat sink configurations introduced. For that purpose, the next cases of study were carried out:

- **CASE 1**: Counter flow – Straight channel configuration
- **CASE 2**: Parallel flow – Straight channel configuration
- **CASE 3**: Counter flow – Zigzag channel configuration
- **CASE 4**: Parallel flow – Zigzag channel configuration

Once we knew the better configuration under the desired working conditions, the melting/solidification model for multi-phase calculations will be applied to it. **Case 2 was chosen as a suitable option to add the MEPCM particles to the working fluid. Therefore, three additional cases were run at different MEPCM particle concentration (10%, 15% and 20%).**

- CASE 2* – 10% MEPCM particle concentration
- CASE 2* – 15% MEPCM particle concentration
- CASE 2* – 20% MEPCM particle concentration

The main results of interest were **temperature** and **pressure** values throughout the channel and at the bottom surface, the one in contact with the heat source. To do so, parameters such as **pressure drop within the channels and the maximum temperature value at the bottom surface** were calculated. It's very important to know the distinct performances that the heat sink designs can offer at different flow rates. For that purpose, additional parameters will be obtained to have a full knowledge of the heat sink behavior:

- **Total thermal resistance**

$$R_{th} = \frac{\Delta T_{max}}{q''}$$

Where **q''** is the applied flux at the base of the heat sink, A_b is the area of the base, and ΔT_{max} is the maximum temperature difference within the heat sink.

$$\Delta T_{max} = T_{b,max} - T_{f,in}$$

Where $T_{b,max}$ is the maximum temperature at the base of the heat sink, and $T_{f,in}$ is the inlet temperature of the coolant liquid. The maximum temperature was chosen as the value defining the thermal resistance because the presence of hot spots will reduce the performance of the micro-chip even though the average value of temperature along the heat sink was low and a good homogeneity would had been obtained [1]. A track on these hot areas was carried out to optimize the heat sink capability.

- **The pumping power**

The pumping power required to pump the fluid through a single micro-channel is given as:

$$P_{ch} = u_{avg} A_c \Delta p_{ch}$$

Where u_{avg} is the average fluid velocity, A_c is the micro-channel cross sectional area, and Δp_{ch} is the pressure drop within a single micro-channel. The total pumping power to pump the fluid is given as:

$$P_{tot} = n P_{ch}$$

Where n is the total number of channels.

- **Dimensionless Temperature and Pressure**

Additionally, to being able to compare among different heat sink designs and channel configurations, the temperature ($\breve{T}$) and pressure ($\breve{P}$) dimensionless variables were defined:

$$\breve{T} = \frac{(T - T_{f,in})}{q'' D_H / k_f}$$

Where D_H is the hydraulic diameter and k_f is the fluid thermal conductivity coefficient. The hydraulic diameter is defined as:

$$D_H = \frac{4A}{P_w}$$

Where **A** is the channel cross sectional area and P_w is the wet perimeter of the channel cross section area.

$$\breve{P} = \frac{(P_{f,in} - P_{f,out}) D_H{}^2}{\alpha_f \mu}$$

Where $\breve{P}$ is the non-dimensional pressure, based on the definition of Petrescu [13] and Bhattacharjee and Grosshandler [14]. α_f is the thermal diffusivity of the fluid and μ is the viscosity.

$$\alpha_f = \frac{k_f}{\rho c_p}$$

- **The Nusselt number**

Additionally, the Nusselt number was calculated as well.

$$\boldsymbol{Nu} = \frac{\boldsymbol{h}\, \boldsymbol{D_H}}{\boldsymbol{k_f}}$$

Where h is the heat transfer coefficient:

$$\boldsymbol{h} = \frac{\mathbf{q}''}{\boldsymbol{\Delta T_{max}}}$$

All these calculations took place within a selected range for the total flow rate. The idea under the heat sink designs shown, or the PCM selected, is to **find the greater cooling enhancement at the lower pumping cost**. For that reason, low flow rates have been selected. Doing so, the total pressure drop, and as a result of it, the total pumping power required by the system will lay within reasonable values. **The total flow rates values went from 0.0005 kg/s till 0.0025 kg/s.**

4.1. MESH INDEPENDENCE STUDY

4.1.1. Single phase fluid

A grid independence test must be carried out to obtain improved accuracy and to cut down the computational cost in both, time and memory, require in the numerical simulations. For this study a rectangular, straight hexahedral mesh was defined for the fluid and the solid volumes. Applying this configuration, it was possible to reduce the number of nodes while enough accuracy could still be reached.

For the independence study, the inlet velocity was specified as **0.5 m/s** (mass flow rate of 5.9892 x 10^{-5} kg/s). As the outputs, the pressure drop along the channel and the maximum temperature at the bottom surface (T_{max}), the one in contact with the heat source, were calculated. The results are shown in table 7.

Table 7 - Grid Independence study (straight channel configuration)

		Mesh I	Mesh II	Mesh III	Mesh IV
Number of nodes		54,873	411,025	836,916	1,126,136
$\boldsymbol{\Delta p}$	Pa	1735.05	1939.19	1978.88	1991.33
$\boldsymbol{T_{max}}$	(K)	328.67	330.50	330.63	330.64
$\boldsymbol{\Delta p}$ **deviation**	(%)		10.53	2.01	0.63
$\boldsymbol{T_{max}}$ **deviation**	(%)		0.55	0.04	0.0045

As it can be inferred, the element´s density of the computational mesh doesn´t have a very significant influence in laminar flow. So, to maintain a proper balance between computational time cost and accuracy, **Mesh III**, with 836,916 nodes, was chosen for all the simulations. The element´s size for the selected grid varies from 5 x 10^{-5} m^3 at the fluid volumes within the channels, to 4.5 x 10^{-4}, approximately, at the solid volume. As shown in figure 6, the simplicity on the geometry allows us to implement a simple hexahedral grid layout.

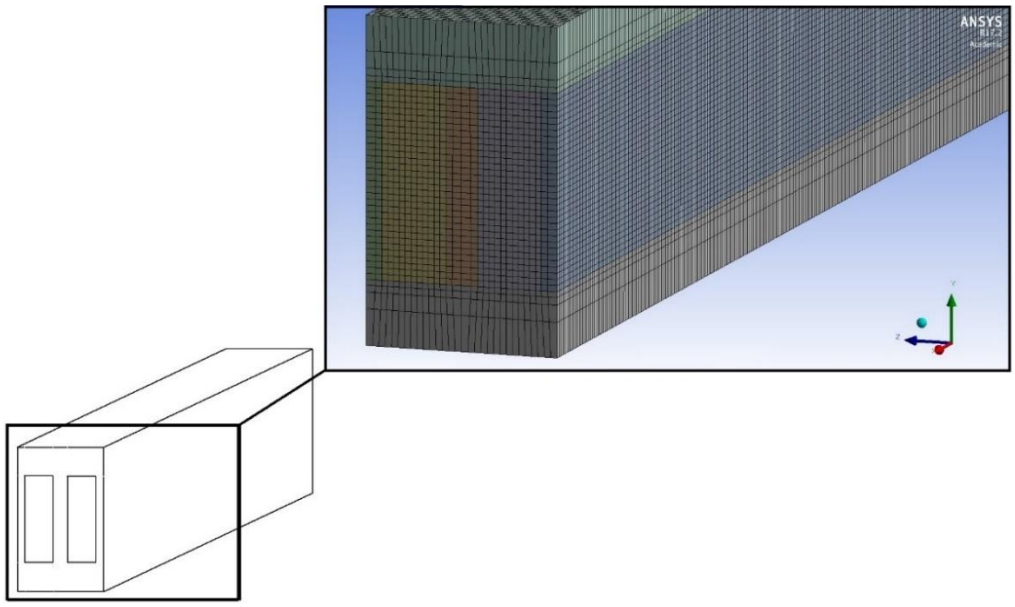

Figure 6 - Mesh III Straight channel configuration

The exact same study was carried out for the zigzag channel configuration:

Table 8 - Grid Independence study (zigzag channel configuration)

		Mesh I	Mesh II	Mesh III	Mesh IV
Number of nodes		122,220	731,293	1,590,208	2,314,385
$\boldsymbol{\Delta p}$	Pa	4659.64	4625.02	4540.9	4535.69
$\boldsymbol{T_{max}}$	(K)	319.25	318.95	319.339	319.342
$\boldsymbol{\Delta p}$ **deviation**	(%)		0.74	1.82	0.11
$\boldsymbol{T_{max}}$ **deviation**	(%)		0.0939	0.1215	0.0008

Where also the **mesh III**, with 1,590,208 nodes was the one used for all calculations. On this case, the element´s size for the selected grid varies from 1 x 10^{-5} m^3 at the fluid volumes within the channels, to 8 x 10^{-4}, approximately, at the solid volume. The zigzag channel configuration implies a greater difficulty for the hexahedral straight elements to adapt to the changing geometry. For that reason, tetrahedral elements were also allowed. Besides, due to the added corners, to keep the same level of accuracy, a reduction of the element´s size was required within the channel. In overall, the same mesh characteristics applied, but with an increase in the number of nodes.

4.1.2. Double phase fluid

Only double phase calculations for the straight channels configuration was carried out. For these cases, as we´ve been working with the temperature transforming model, which is independent of the grid size, basically the same grid density was used. However, a better-quality grid elements distribution was performed. As we were working with additional functions hooked to fluent, a refinement was necessary to reduce the computational time as much as possible. Keeping the same grid configuration, a slightly reduction in the element´s size within the channel, and a higher growth ratio at the solid volume was implemented. Eventually, these modifications on the **mesh III**, used for the previous single phase calculations, increased the total number of nodes till 990,478. On this new modified grid, **mesh III***, the element´s size for the selected grid varies from 1.9 x 10^{-5} m^3 at the fluid volumes within the channels, to 1.5 x 10^{-4}, approximately, at the solid volume.

4.2. SINGLE PHASE

The results for the first four cases of study are shown below. Cases 1-2, firstly, and cases 3-4, secondly, are going to be presented together. Straight and zigzag channel configurations were analyzed separately and, eventually, final conclusions regarding ''counter-parallel'' flow and ''straight-zigzag'' channel configuration are discussed.

4.2.1. STRAIGHT CHANNELS - Case 1 & 2

4.2.1.a. Heat Sink performance values

The first two cases under study correspond to the straight channel configuration. The parameters of interest, as discuss previously, are shown below in table 9 and 10, respectively for counter and parallel flow configuration.

Table 9 - Single phase - Straight channels, counter flow

Total flow rate	(kg/s)	**0.0005**	**0.001**	**0.0015**	**0.002**	**0.0025**
Flow rate per channel	(kg/s)	1.52E-05	3.03E-05	4.55E-05	6.06E-05	7.58E-05
v	(m/s)	0.126	0.253	0.379	0.506	0.632
Total Pressure inlet	(Pa)	490.59	1018.39	1571.78	2170.28	2784.85
Total Pressure outlet	(Pa)	10.64	42.03	93.76	166.45	259.19
$T_{s,max}$	(K)	363.64	341.46	334.33	330.53	328.04
u_{avg}	(m/s)	0.126	0.253	0.379	0.506	0.632
P_{ch}	(watt)	7.26E-06	2.96E-05	6.72E-05	1.22E-04	1.92E-04
P_{tot}	(watt)	2.39E-04	9.78E-04	2.22E-03	4.02E-03	6.32E-03
Δp_{ch}	(Pa)	479.95	976.36	1478.02	2003.83	2525.66
ΔT_{max}	(K)	63.64	41.46	34.33	30.53	28.04
R_{th}	(Km^2/W)	6.36E-05	4.15E-05	3.43E-05	3.05E-05	2.80E-05
$\breve{T}_{max}$		0.129	0.084	0.069	0.062	0.057
$\Delta\breve{P}_{ch}$		2.93E+05	5.97E+05	9.04E+05	1.23E+06	1.54E+06
Nu		7.77	11.92	14.40	16.19	17.63

Table 10 - Single phase - Straight channels, parallel flow

Total flow rate	(kg/s)	**0.0005**	**0.001**	**0.0015**	**0.002**	**0.0025**
Flow rate per channel	(kg/s)	1.52E-05	3.03E-05	4.55E-05	6.06E-05	7.58E-05
v	(m/s)	0.126	0.253	0.379	0.506	0.632
Total Pressure inlet	(Pa)	490.59	1018.39	1571.75	2170.28	2784.87
Total Pressure outlet	(Pa)	10.64	42.03	93.76	166.45	259.24
$T_{s,max}$	(K)	365.70	344.08	336.58	332.47	329.79
u_{avg}	(m/s)	0.126	0.253	0.379	0.506	0.632
P_{ch}	(watt)	7.26E-06	2.96E-05	6.72E-05	1.22E-04	1.92E-04
P_{tot}	(watt)	2.39E-04	9.78E-04	2.22E-03	4.02E-03	6.32E-03
Δp_{ch}	(Pa)	479.95	976.36	1477.99	2003.83	2525.63
ΔT_{max}	(K)	65.70	44.08	36.58	32.47	29.79
R_{th}	(Km^2/W)	6.57E-05	4.41E-05	3.66E-05	3.25E-05	2.98E-05
$\breve{T}_{max}$		0.133	0.089	0.074	0.066	0.060
$\Delta\breve{P}_{ch}$		2.93E+05	5.97E+05	9.04E+05	1.23E+06	1.54E+06
Nu		7.52	11.21	13.51	15.22	16.59

4.2.1.b. Overall thermal-performance

Apart of the numerical values, to illustrate the behavior and tendencies of this parameters with the variation on the total flow rate, the next graphs concerning the total pressure drop along the channels, the maximum temperature reached at the bottom surface, and global performance parameters such as the global thermal resistance and the dimensionless pressure drop, are presented below in figure 7.

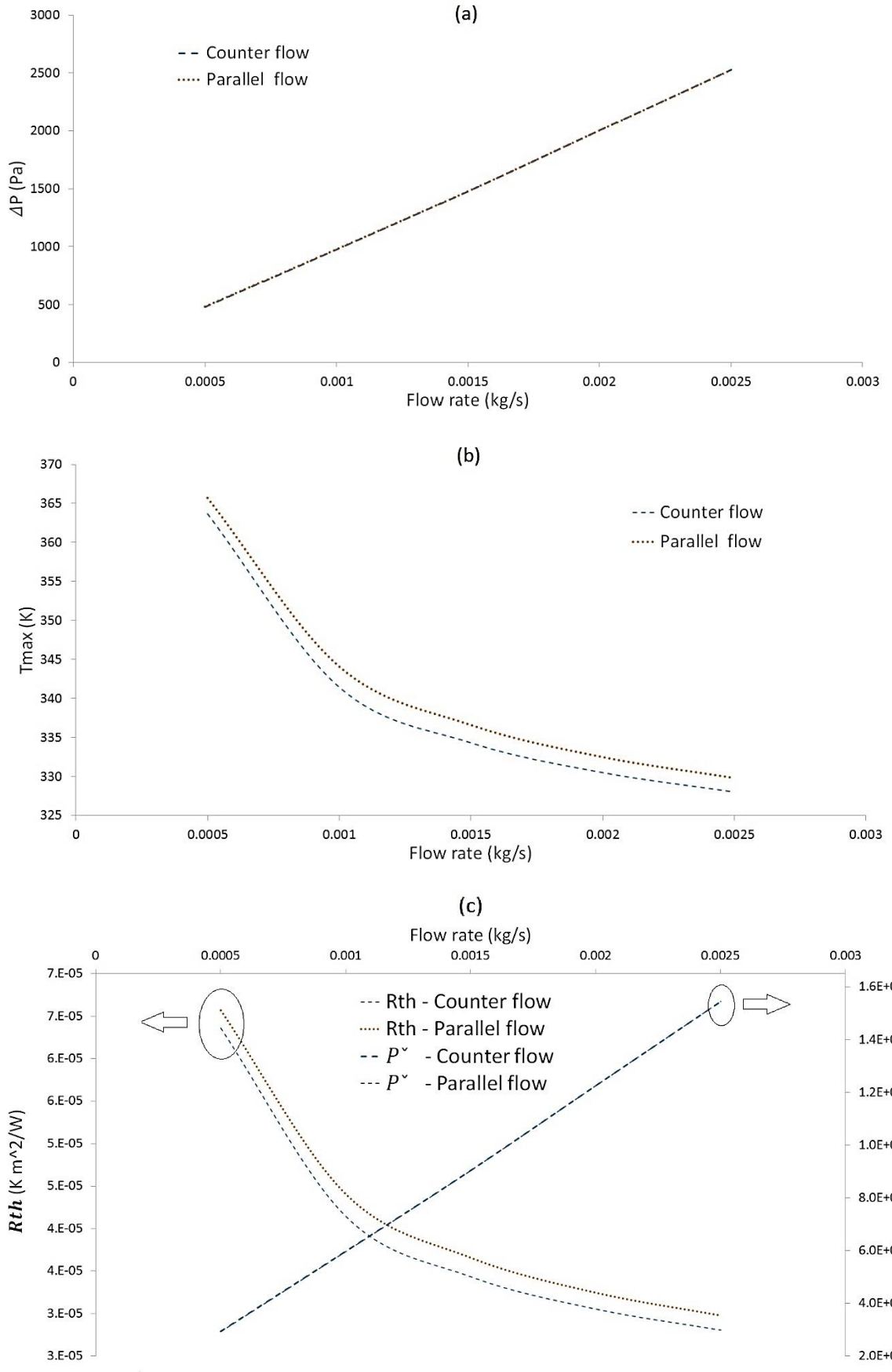

Figure 7 - Variations of (a) total pressure drop, (b) max. bottom surface temperature, and (c) dimensionless pressure drop and thermal resistance with total flow rate in counter and parallel flow with straight channel configuration

Where, as it can be inferred, the total pressure drop increases linearly with the inlet velocity. The channel geometry configuration is identical, so the same values for pressure were obtained. So, higher values of total flow lead to a linear growth in pressure drop, however the reduction in temperature at the heat source surface varies in an exponential way. The enhancement in thermal-performance will be more notable at lower flow rates than at higher values, where a bigger increment in energy will be required to pump the fluid through the channels for a lower decrease in the maximum temperature reached.

At the same total flow rate, a better thermal behavior is observed for counter flow configuration; keeping, always, the bottom surface cooler than the parallel flow configuration. This positive aspect, together with a better homogeneity in temperature (due to the intrinsic nature of its design), suggests counter flow configuration as a better option with regard to these overall parameters.

Finally, the same tendencies can be observed in figure 7.c for the thermal resistance and the dimensionless pressure drop.

Combining these two-main overall heat sink performance parameters (maximum temperature reached at the bottom and total pressure drop), it is possible to show the real heat sink performance in terms of energy applied to the system related to the maximum thermal enhancement provided, figure 8. These values correspond to the thermal resistance per total pumping power required; where, once more, counter flow configuration shows a better capability to cool down the system, even at a lower energy cost.

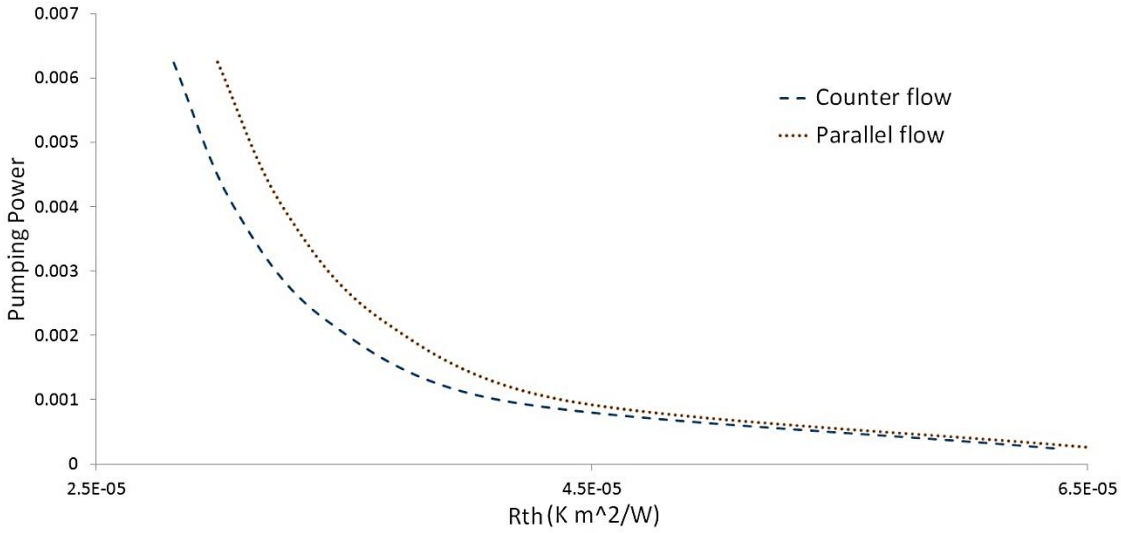

Figure 8 - Thermal resistance related to the pumping power required by the system for straight channel configuration

4.2.1.c Heat sink behavior throughout the channels

Once the overall performance has been discussed, let´s analyze the behavior that the two different flow configurations offer along the longitudinal direction. For that purpose, some additional graphs regarding the mean temperature distribution throughout the fluid channel and bottom surface will be shown below in figure 9. **Just temperature distributions for three out of the five total flow rates values selected will be shown**. This will be sufficient to show the evolution in temperature tendencies with the increase in the flow rate.

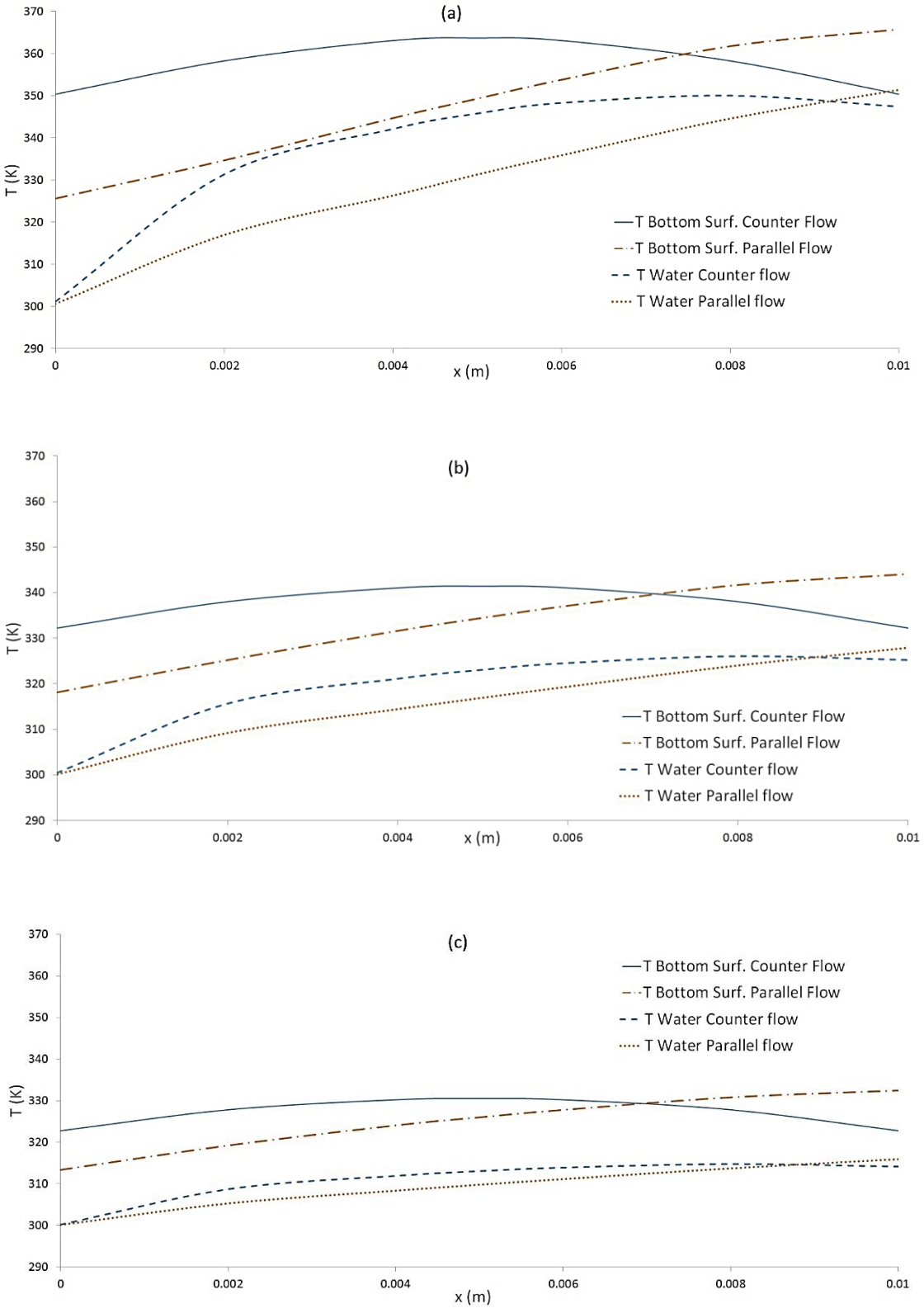

Figure 9 - Mean temperature distribution throughout the fluid channel and the bottom surface at (a) 0.0005, (b) 0.001 and (c) 0.002 kg/s in counter and parallel flow with straight channel configuration

Where the fluid temperature values shown correspond to just one of the two channels. The predicted overall reduction in temperature with the increment in the total flow rate can be observed. Meanwhile the **parallel flow configuration shows an almost linear increment in both, fluid and bottom surface temperature along the x direction**; the **counter flow gets to keep a more regular and homogenous temperature distribution** at the bottom surface and within the channel.

However, in opposition to the clear improvement in the overall parameters shown before, now it is clear that, even though the parallel flow configuration offered a higher thermal resistance, a higher percentage of the total heat sink body works at a lower temperature. Also, the mean temperature of the working fluid throughout the channel is kept at a lower temperature, which means a higher capacity to absorb heat. These differences diminish with the increase in the total flow rate.

Additionally, contour plots for pressure and temperature distribution, and velocity profiles were added for the better understanding of these two flow configurations**. In an effort to fully illustrate the heat sink behavior, but trying to avoid to overwhelm the lector with too many contours images, just two flow rates were selected for all cases (0.0005 and 0.002 kg/s).**

- Bottom surface temperature distribution:

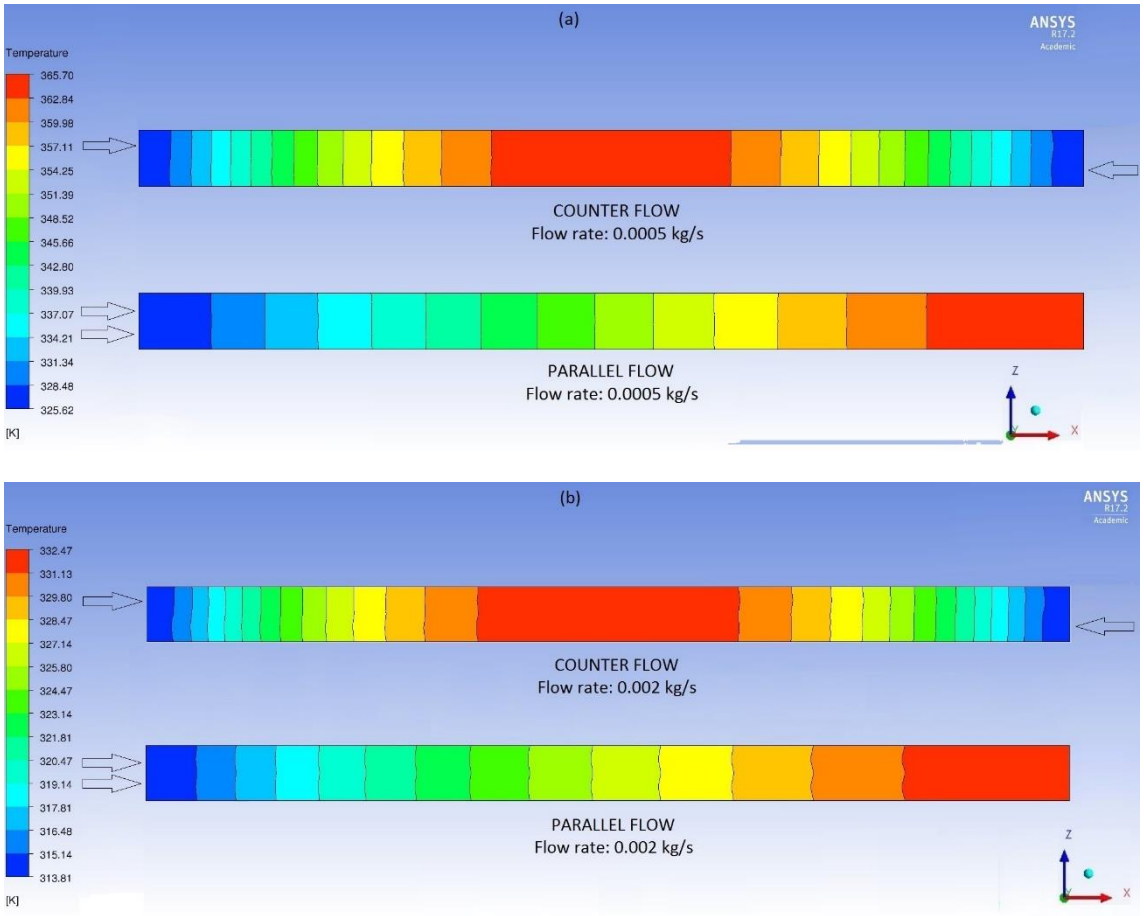

Figure 10 - Temperature contours at the bottom surface at (a) 0.0005 and (b) 0.002 kg/s in counter and parallel flow with straight channel configuration

Where the arrows show the direction of the flow in both cases. The same view configuration will be kept, so no more arrows will be shown.

Here it is more clear to see the better homogeneity that counter flow configuration provides to the system in contrast to the higher temperature difference between inlet and outlet for parallel flow. However, on this second case, just the end of the channel will be put down to a high temperature. And what is more, the part of heat sink under undesirable values of temperature for parallel flow configuration seems to be less in comparison with the counter flow.

- Vertical symmetry plane temperature distribution:

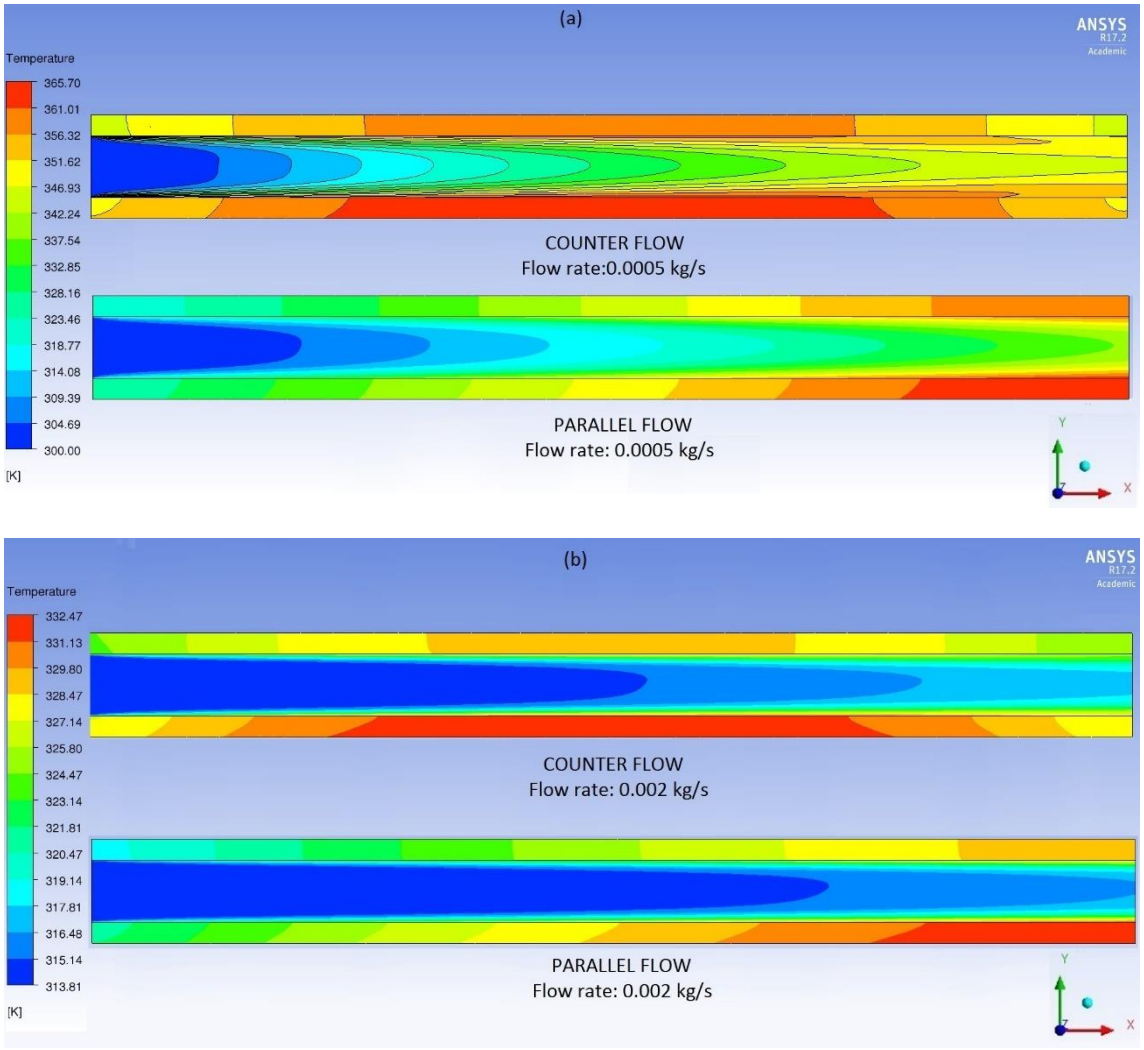

Figure 11 - Temperature contours throughout the vertical symmetry plane at (a) 0.0005 and (b) 0.002 kg/s in counter and parallel flow with straight channel configuration

Regarding the fluid temperature distribution throughout the channel, the differences between counter and parallel flow configuration decrease. Counter flow reaches higher temperatures faster and in shorter distance than parallel flow. **This fact was taken into consideration when selecting the PCM particle melting range.** The cooling system ought to be designed so that the MEPCM particles start melting at the channel inlet and they should be completely melted by the time the particles reach the channel exit [8].

- Vertical symmetry plane pressure distribution:

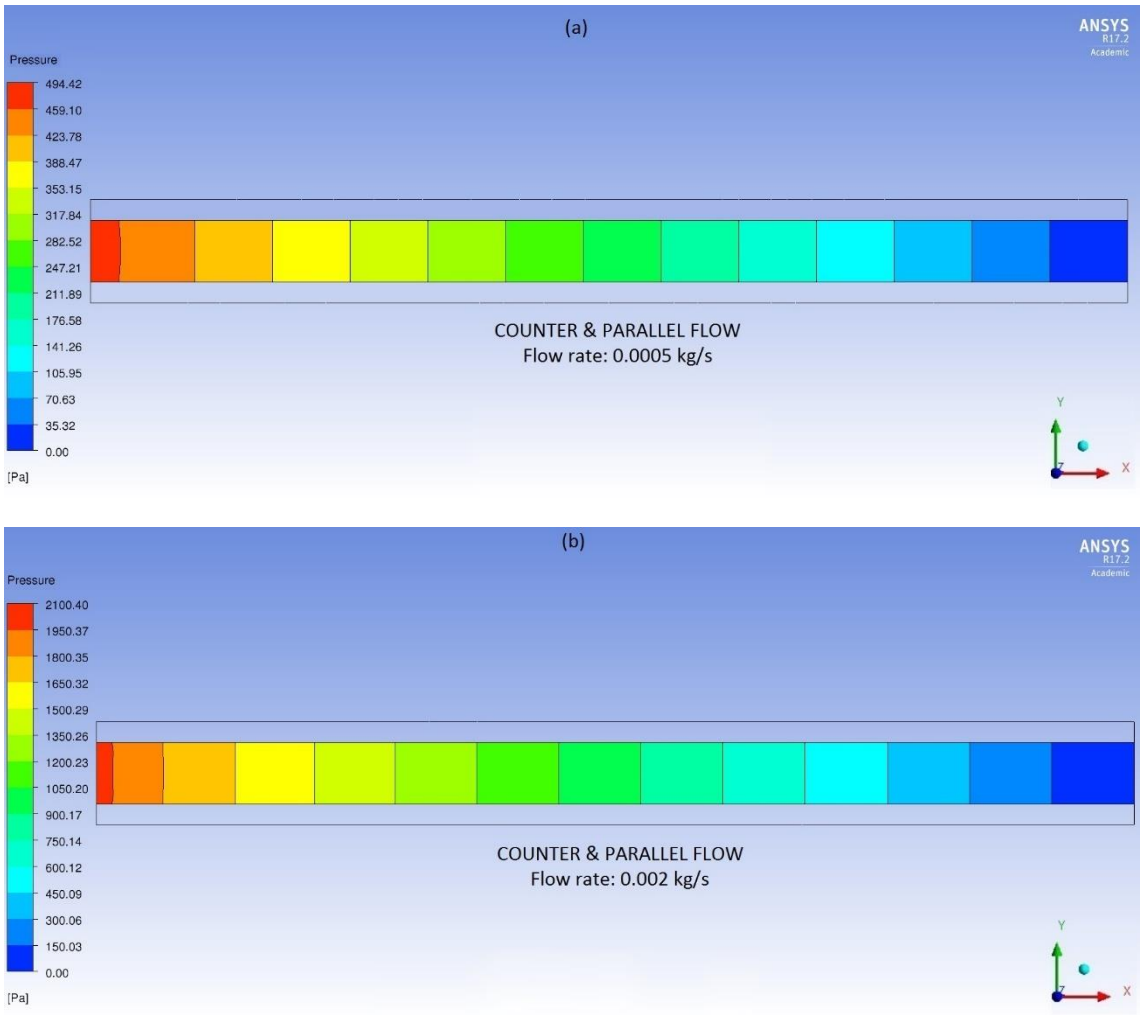

Figure 12 - Pressure contours throughout the vertical symmetry plane at (a) 0.0005 and (b) 0.002 kg/s in counter and parallel flow with straight channel configuration

Same distribution along the channel for both flow configurations is seen. This distribution behavior is also kept when increasing the flow rate.

- Vertical symmetry plane velocity distribution:

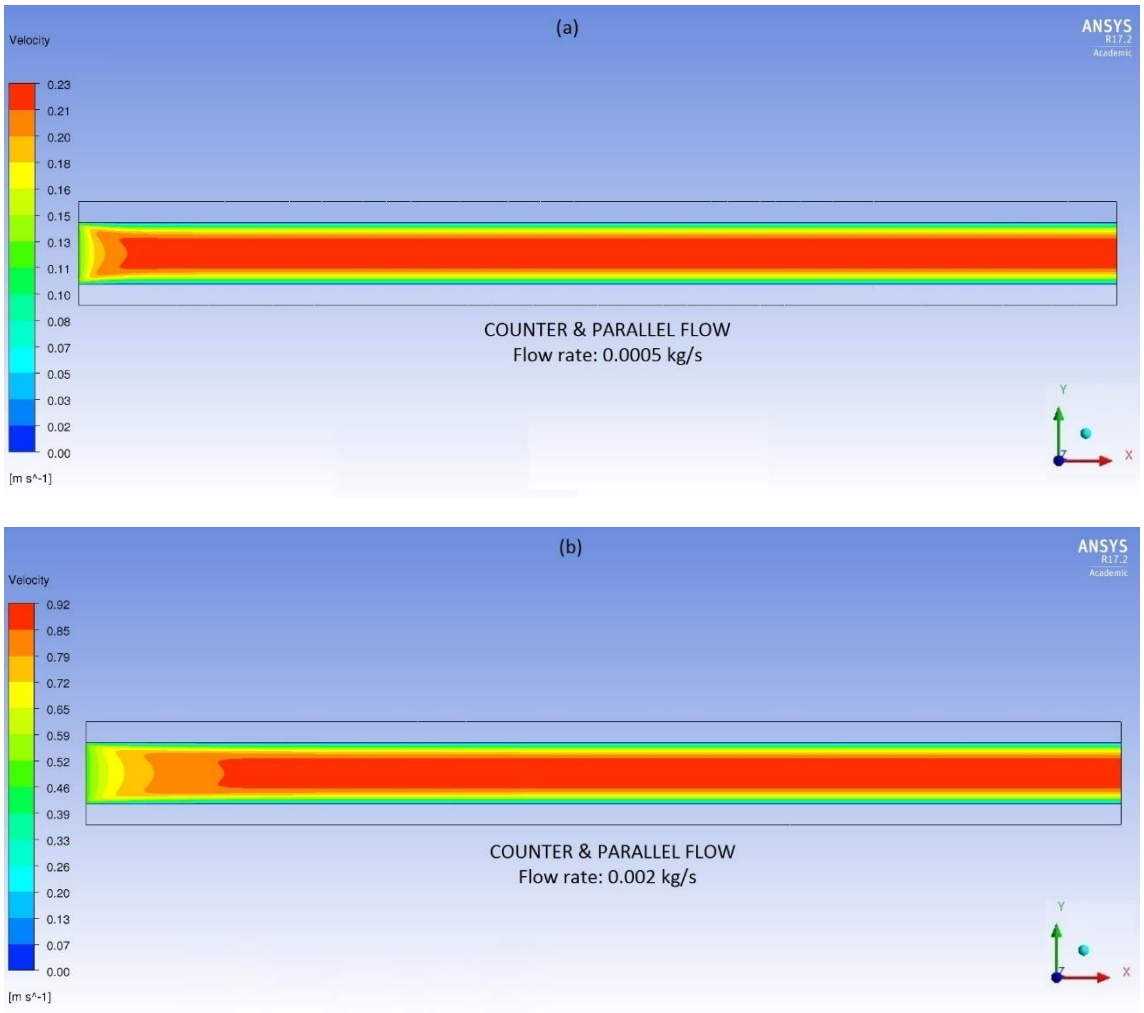

Figure 13 - Velocity contours throughout the vertical symmetry plane at (a) 0.0005 and (b) 0.002 kg/s in counter and parallel flow with straight channel configuration

Finally, the velocity profiles distribution is shown, where similar tendencies are observed. The fluid gets fully developed at different x values for different inlet velocity values. Also, the boundary layer gets thicker at higher velocities due to the increment in Reynolds' number value.

4.2.2. ZIGZAG CHANNELS - Case 3 & 4

4.2.2.a. Heat Sink performance values

The next two cases correspond to the zigzag channel configuration. The same parameter values than before are shown below in Table 11 and 12, respectively for counter and parallel flow configuration.

Table 11 - Heat sink performance values – Counter flow zigzag channels

Total flow rate	(kg/s)	**0.0005**	**0.001**	**0.0015**	**0.002**	**0.0025**
Flow rate per channel	(kg/s)	1.52E-05	3.03E-05	4.55E-05	6.06E-05	7.58E-05
v	(m/s)	0.126	0.253	0.379	0.506	0.632
Total Pressure inlet	(Pa)	775.59	1820.96	3007.03	4825.09	6802.11
Total Pressure outlet	(Pa)	10.64	42.09	93.89	165.46	258.42
$T_{s,max}$	(K)	359.99	335.82	327.03	322.16	319.96
u_{avg}	(m/s)	0.136	0.273	0.408	0.545	0.681
P_{ch}	(watt)	1.25E-05	5.83E-05	1.43E-04	3.05E-04	5.35E-04
P_{tot}	(watt)	4.13E-04	1.92E-03	4.71E-03	1.00E-02	1.76E-02
Δp_{ch}	(Pa)	764.95	1778.87	2913.13	4659.63	6543.69
ΔT_{max}	(K)	59.99	35.82	27.03	22.16	19.96
R_{th}	(Km^2/W)	6.00E-05	3.58E-05	2.70E-05	2.22E-05	2.00E-05
$\breve{T}_{max}$		0.121	0.072	0.055	0.045	0.040
$\Delta\breve{P}_{ch}$		4.68E+05	1.09E+06	1.78E+06	2.85E+06	4.00E+06
Nu		8.24	13.80	18.29	22.31	24.77

Table 12 - Heat sink performance values – Parallel flow zigzag channels

Total flow rate	(kg/s)	**0.0005**	**0.001**	**0.0015**	**0.002**	**0.0025**
Flow rate per channel	(kg/s)	1.52E-05	3.03E-05	4.55E-05	6.06E-05	7.58E-05
v	(m/s)	0.126	0.253	0.379	0.506	0.632
Total Pressure inlet	(Pa)	775.59	1820.96	3007.28	4825.09	6802.11
Total Pressure outlet	(Pa)	10.64	42.09	93.88	165.47	258.42
$T_{s,max}$	(K)	361.51	339.05	330.00	325.33	323.00
u_{avg}	(m/s)	0.136	0.273	0.408	0.545	0.681
P_{ch}	(watt)	1.25E-05	5.83E-05	1.43E-04	3.05E-04	5.35E-04
P_{tot}	(watt)	4.13E-04	1.92E-03	4.71E-03	1.00E-02	1.76E-02
Δp_{ch}	(Pa)	764.95	1778.87	2913.40	4659.63	6543.69
ΔT_{max}	(K)	61.51	39.05	30.00	25.33	23.00
R_{th}	(Km^2/W)	6.15E-05	3.91E-05	3.00E-05	2.53E-05	2.30E-05
$\check{T}_{max}$		0.124	0.079	0.061	0.051	0.047
$\Delta\check{P}_{ch}$		4.68E+05	1.09E+06	1.78E+06	2.85E+06	4.00E+06
Nu		8.04	12.66	16.48	19.52	21.49

The same procedure than for case 1,2 to graphically show all results was followed

.

4.2.2.b. Overall thermal-performance

The total pressure drop along the channels, the maximum temperature reached at the bottom surface, and global performance parameters such as the global thermal resistance and the dimensionless pressure drop, are presented below in figure 15.

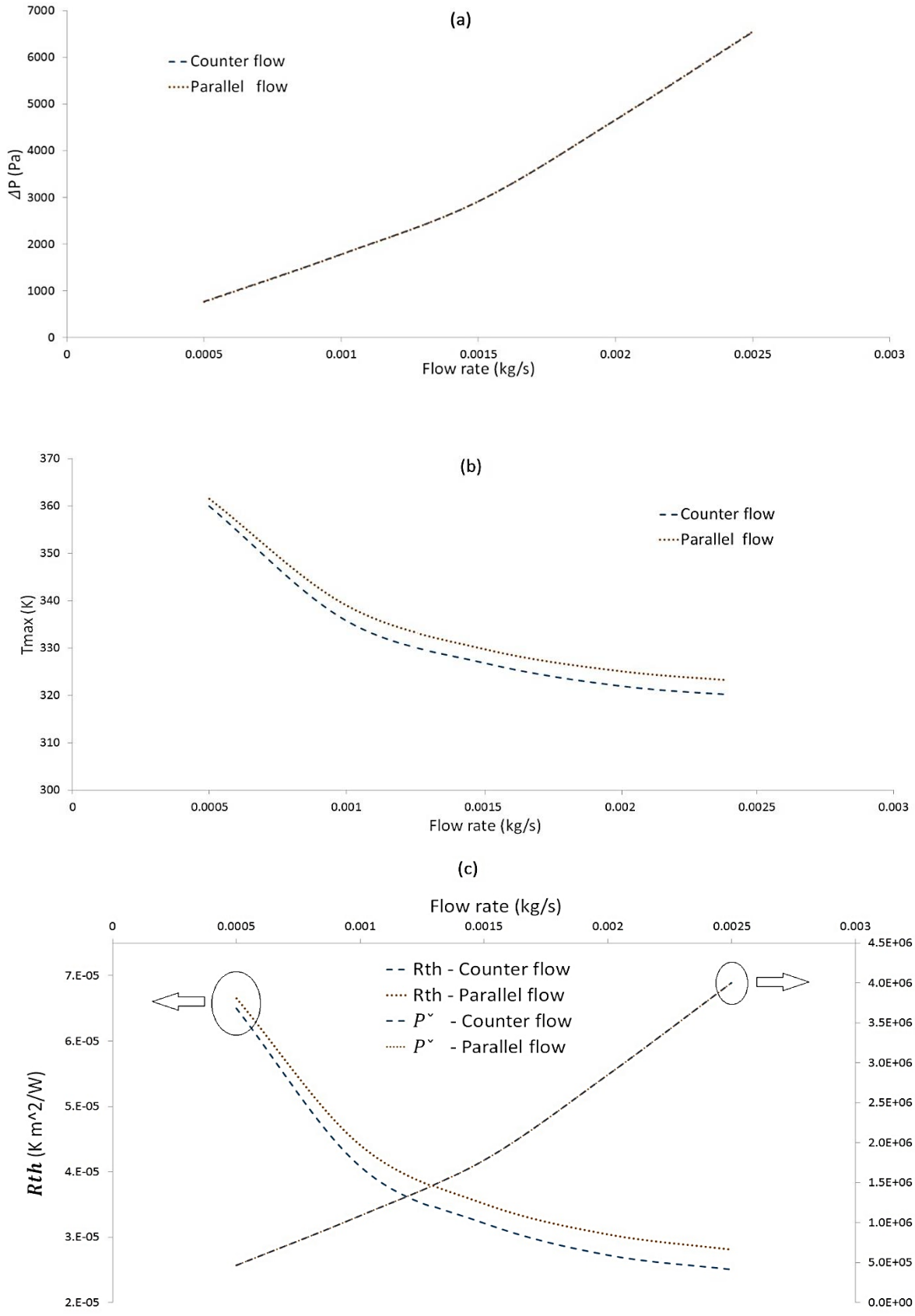

Figure 14 - Variations of (a) total pressure drop, (b) max. bottom surface temperature, and (c) dimensionless pressure drop and thermal resistance with total flow rate in counter and parallel flow with Zigzag channel configuration

Where, following a similar tendency, higher pressure values, at all flow rates, are obtained. The previous linearity observed is, somehow, kept till total flow rate values of 0.0015 kg/s. After that, the slope increases considerably. Temperature maximum values maintain the same behavior than for cases 1 and 2 with flow rate, but with a notable decrease. Counter flow stays as the best cooler regarding the overall parameters.

The thermal resistance per total pumping power required for case 3 and 4 is also shown in figure 16:

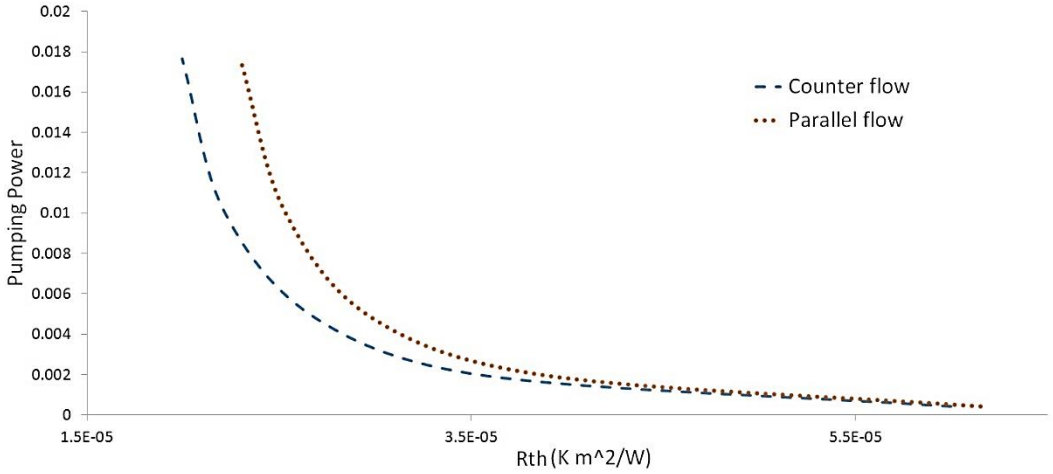

Figure 15 - Thermal resistance related to the pumping power required by the system for zigzag channel configuration

4.2.2.c. Heat sink behavior throughout the channels

The mean temperature distribution throughout the fluid channel and bottom surface is shown below in figure 17.

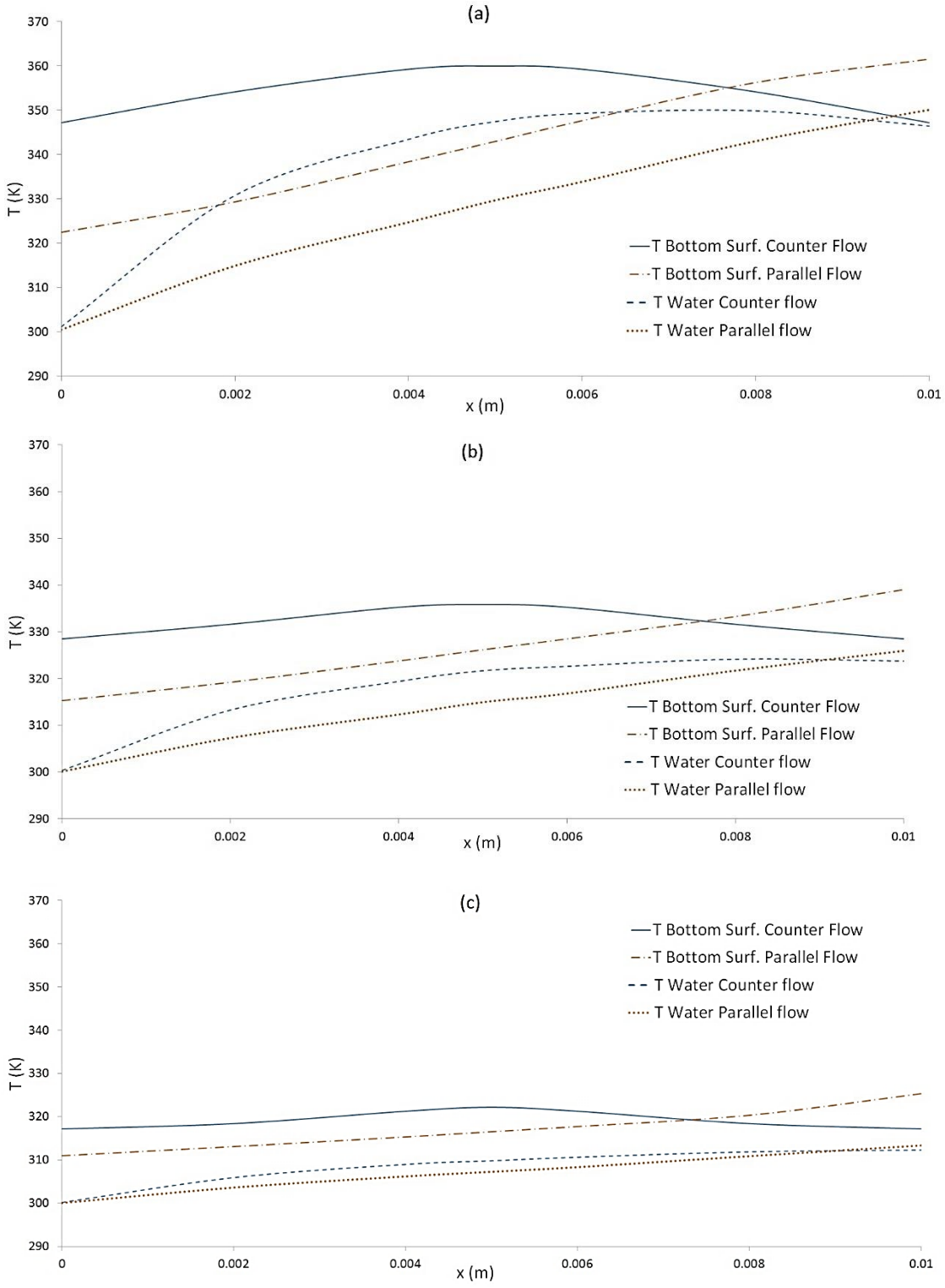

Figure 16 - Mean temperature distribution throughout the fluid channel and the bottom surface at (a) 0.0005, (b) 0.001 and (c) 0.002 kg/s in counter and parallel flow with zigzag channel configuration

Where same tendencies than for cases 1,2 can be deduced.

The contour plots for pressure and temperature distribution, and velocity profiles will be added below:

- Bottom surface temperature distribution:

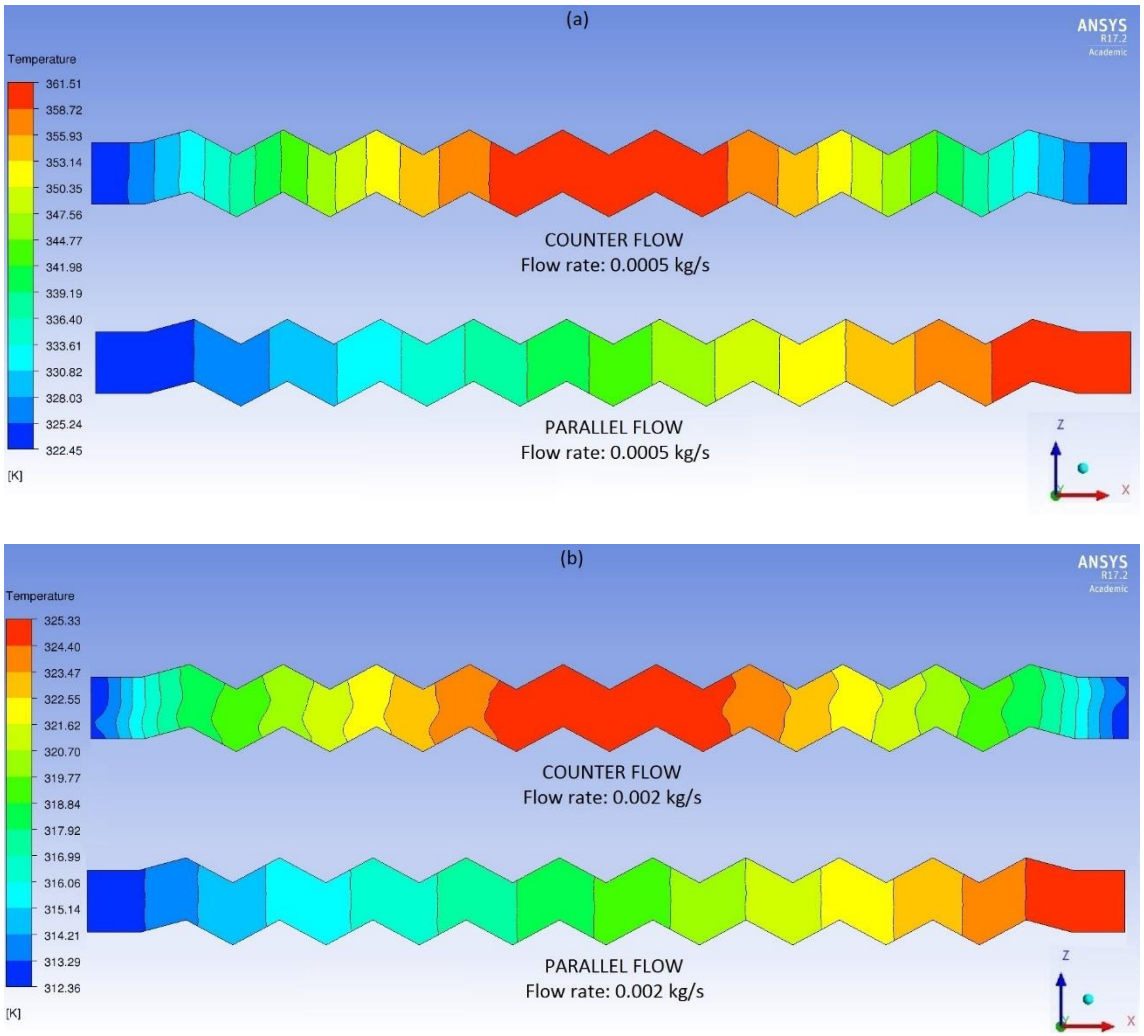

Figure 17 - Temperature contours at the bottom surface at (a) 0.0005 and (b) 0.002 kg/s in counter and parallel flow with Zigzag channel configuration

Where same direction of the flow is kept. No more arrows will be shown.

- Vertical symmetry plane temperature distribution:

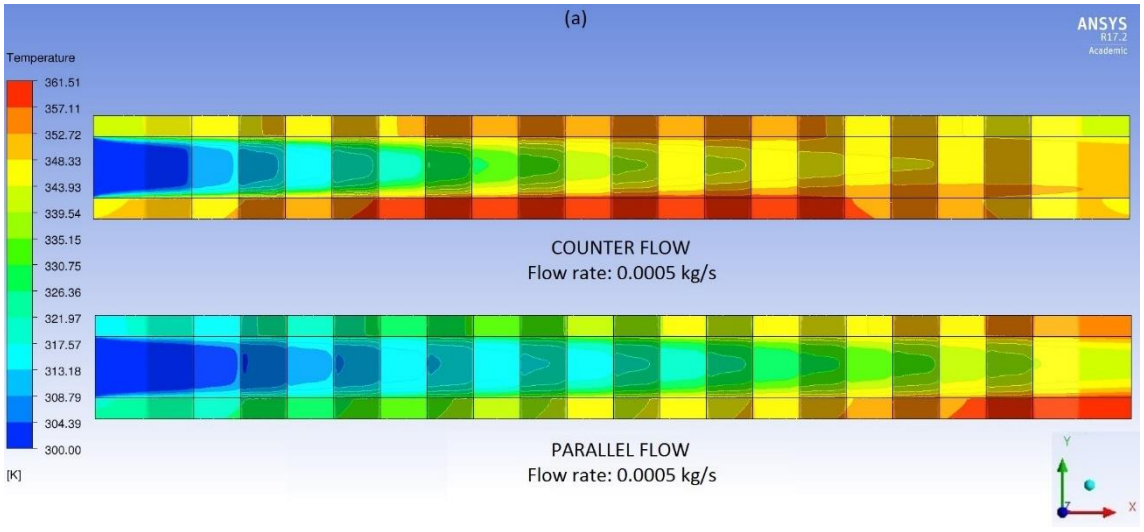

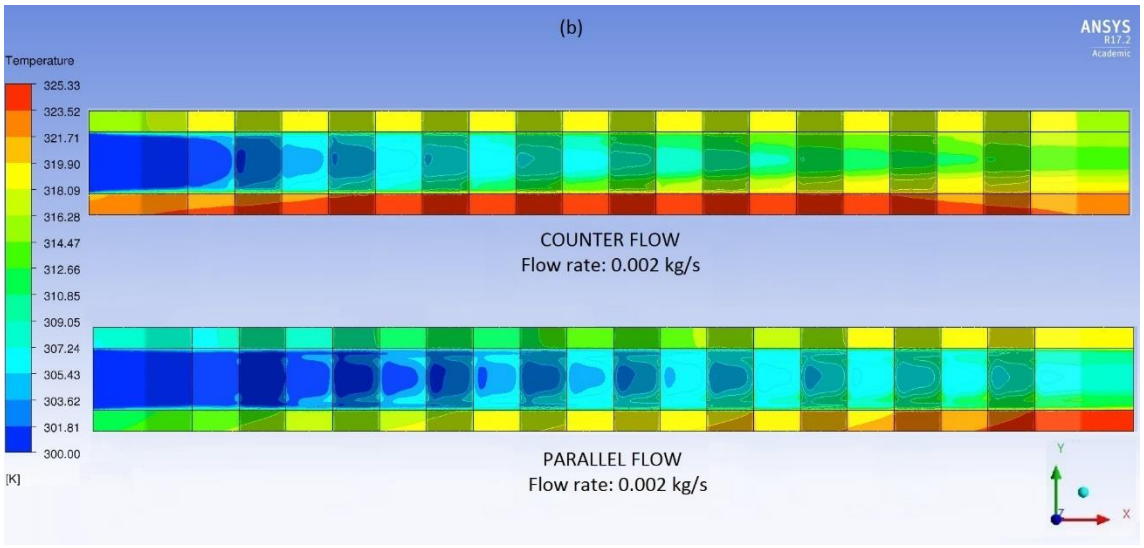

Figure 18 -Temperature contours throughout the vertical symmetry plane at (a) 0.0005 and (b) 0.002 kg/s in counter and parallel flow with Zigzag channel configuration

- Vertical symmetry plane pressure distribution:

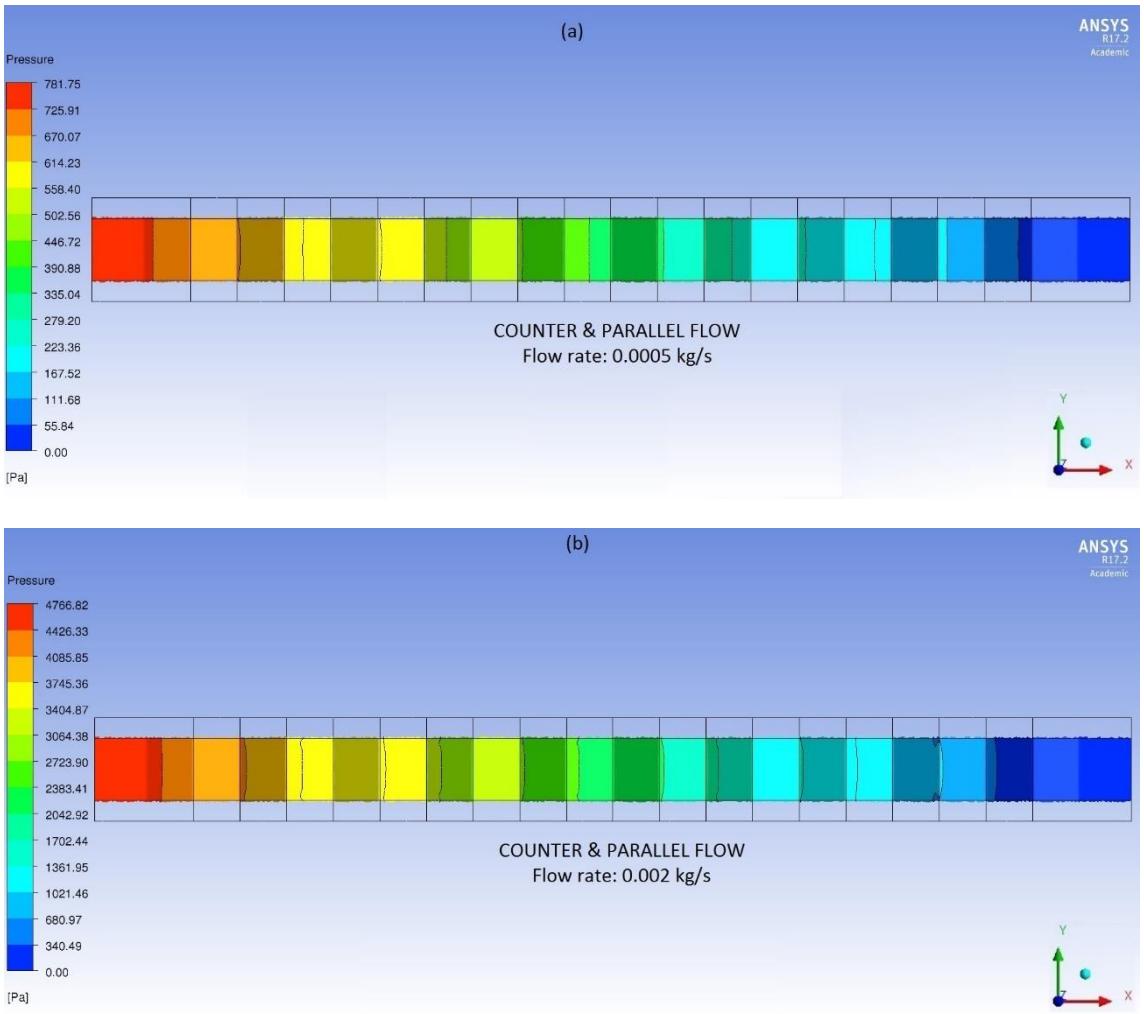

Figure 19 - Pressure contours throughout the vertical symmetry plane at (a) 0.0005 and (b) 0.002 kg/s in counter and parallel flow with Zigzag channel configuration

- Vertical symmetry plane velocity distribution:

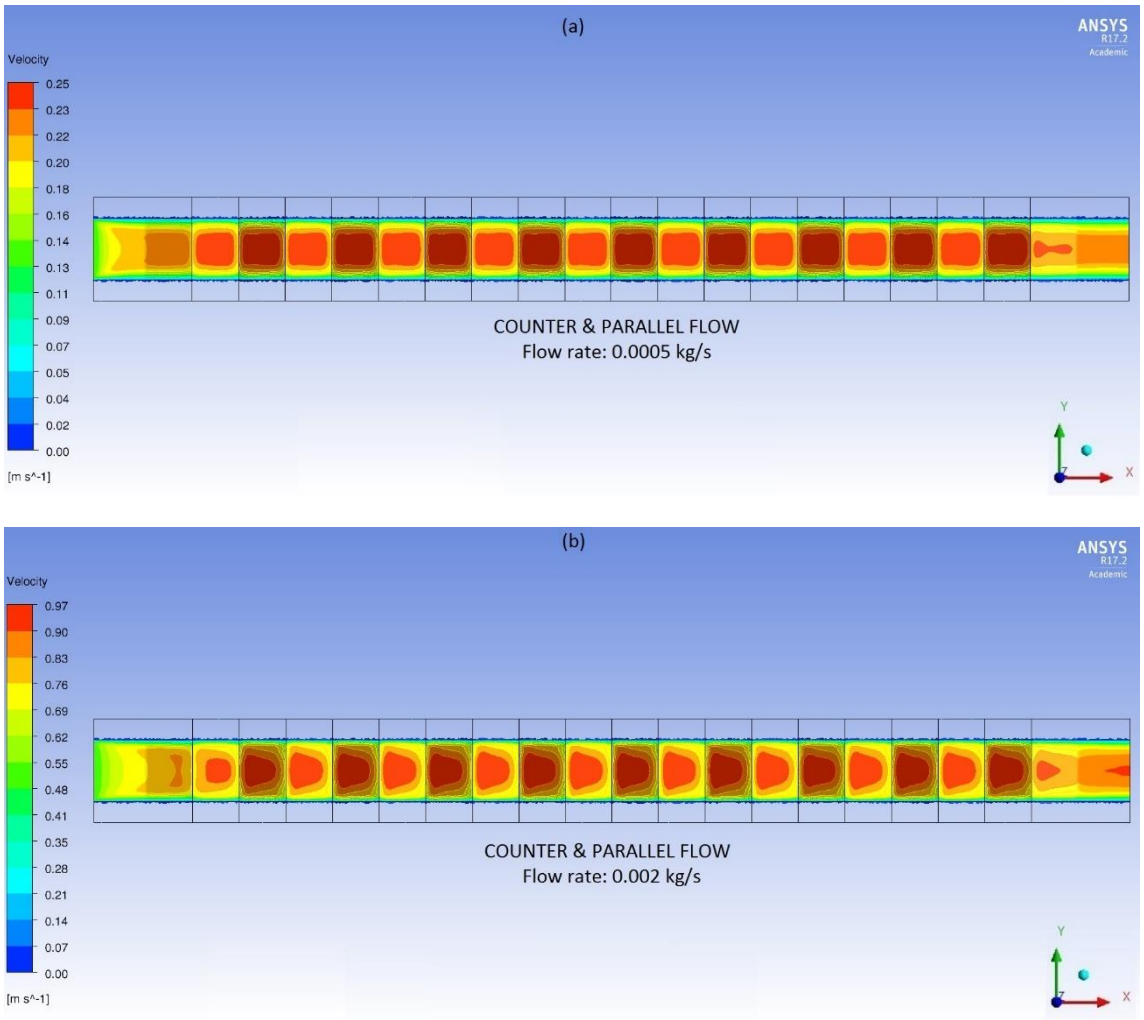

Figure 20 - Velocity contours throughout the vertical symmetry plane at (a) 0.0005 and (b) 0.002 kg/s in counter and parallel flow with Zigzag channel configuration

Being, on this case, harder to visualize the velocity development along the channel. For that reason, an additional view will be added. The next contour plots show the velocity distribution from a horizontal symmetry plane. **The images correspond to counter flow configuration, however, the velocity distribution throughout a single channel is going to be the same regardless the flow configuration applied.**

- Horizontal symmetry plane velocity distribution:

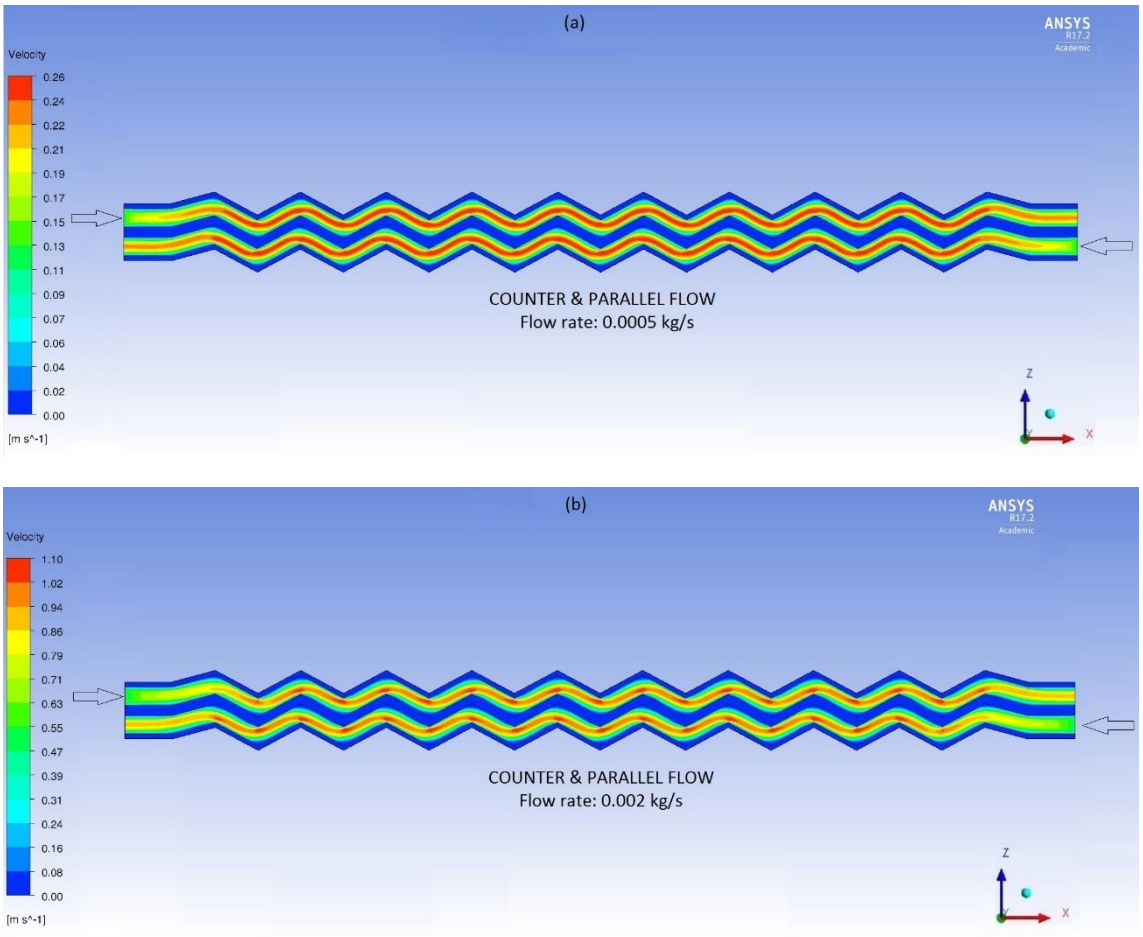

Figure 21 - Velocity contours throughout the horizontal symmetry plane at (a) 0.0005 and (b) 0.002 kg/s in counter and parallel flow with Zigzag channel configuration

It is obvious that the zigzag channel configuration provides a completely different velocity distribution along the channels. Trying, the fluid, to adapt itself to the geometry, higher velocity spots are found over every corner of the zigzags. These increments in velocity will provide a different cooling behavior compared to the straight channel configuration.

4.2.3. PARALLEL – COUNTER FLOW CONFIGURATION ANALYSIS

To analyze the better configuration for applying the phase change model, two parallel analysis were carried out, regarding ''parallel-counter'' flow, and ''straight-zigzag'' configuration. The first of those, **applied to the straight channel configuration**, is discuss in this section. The results for the zig zag channel configuration, as seen before, are similar.

Referring to the figures 8 and 9, where the values of the thermal resistance, and the mean temperature distribution throughout the bottom surface are shown, respectively; the next conclusions can be obtained.

First of all, taking an overlook to the values for the thermal resistance at different flow rates, **the counter flow presents a better overall performance at all flow rates**. Taking closer values both configurations when the flow rate gets closer to 0.0005 kg/s and below. In the next table, it is possible to observed the differences in thermal resistance percentage between the two configurations.

Table 13 - Difference between parallel and counter flow thermal resistance values

Total flow rate	**0.0005**	**0.001**	**0.0015**	**0.002**	**0.0025**
DeviatioN (%)	0.73	1.85	3.54	4.69	5.08

On the other hand, in figure 9 it is possible to observe that even though the maximum value of temperature at the bottom surface is higher for the parallel flow configuration, this difference is relatively small in temperature difference, at a flow rate of 0.0005 kg/s is just **0.563%. For parallel flow configuration, almost all along the channel, the bottom surface temperature is kept under the minimum temperature value provided by the counter flow configuration**. Still for a flow rate of 0.0005 kg/s, the differences in temperature at the front and back surface of the heat sink are **7.05%** higher for the counter flow configuration at the inlet, and just **4.21%** higher for the parallel flow at the outlet. So, one can concluded that **parallel flow configuration provides a better temperature distribution over the heat sink body**.

Another positive aspect that the **counter flow configuration** provides is a **better temperature homogeneity at the bottom surface.**

Similar results are obtained for the rest of the cases, and for zigzag channels configuration. Being the parallel flow performance even better for the zigzag channels configuration in comparison to the counter flow.

So, in overall, both configurations provide similar results as one increase the total flow rate. Considering the maximum value of temperature reached, the counter flow configuration offers a slightly better cooling performance, with a better homogeneity in temperature at the bottom surface. However parallel flow provides better results cooling down the heat sink to lower values than the counter flow configuration does for most the heat sink body.

4.2.4. STRAIGHT – ZIGZAG CHANNEL CONFIGURATION ANALYSIS

For this analysis results for **parallel flow configuration will be used**. First, let's compare the maximum temperature values at the bottom surface between these two-channel configurations. Figure 23.

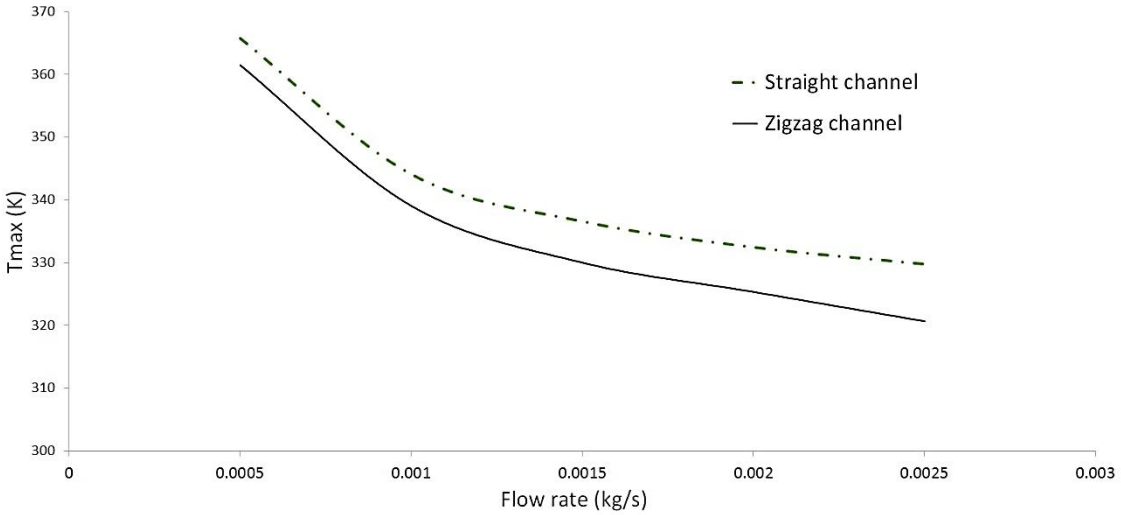

Figure 22 - Variations of max. bottom surface temperature with total flow rate in parallel flow with straight and zigzag channel configuration

Where the maximum difference in temperature over a flowrate of 0.0025 kg/s is **2.98%**. Cooling performance is clearly better for zigzag channels configuration, however this enhancement in temperature is small compare with the increase in pressure drop with flow rate, figure 24.

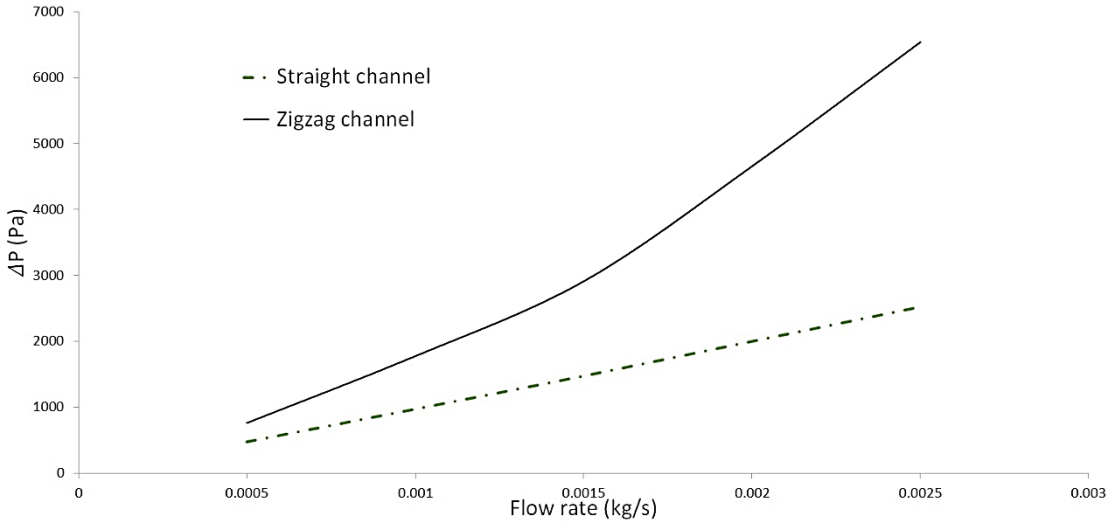

Figure 23 - Variations of total pressure drop throughout the channels with total flow rate in parallel flow with straight and zigzag channel configuration

Where the maximum difference in total pressure corresponds to **61.4%** at 0.0025 kg/s.

So, in terms of efficiency, the increase in the values of pressure drop does not compensate the enhance in temperature that the zigzag channel configuration provides. **The straight channel configuration offers a pretty good thermal-performance with a minimum drop in the total pressure compare to the zigzag configuration.**

Another parameter that could be interesting is the heat transfer coefficient, which increases with the flowrate for both cases. However, the difference for this value between straight and zigzag channel configuration also increases at higher flowrates. Another way to show this same tendency is with the nusselt number. Figure 25.

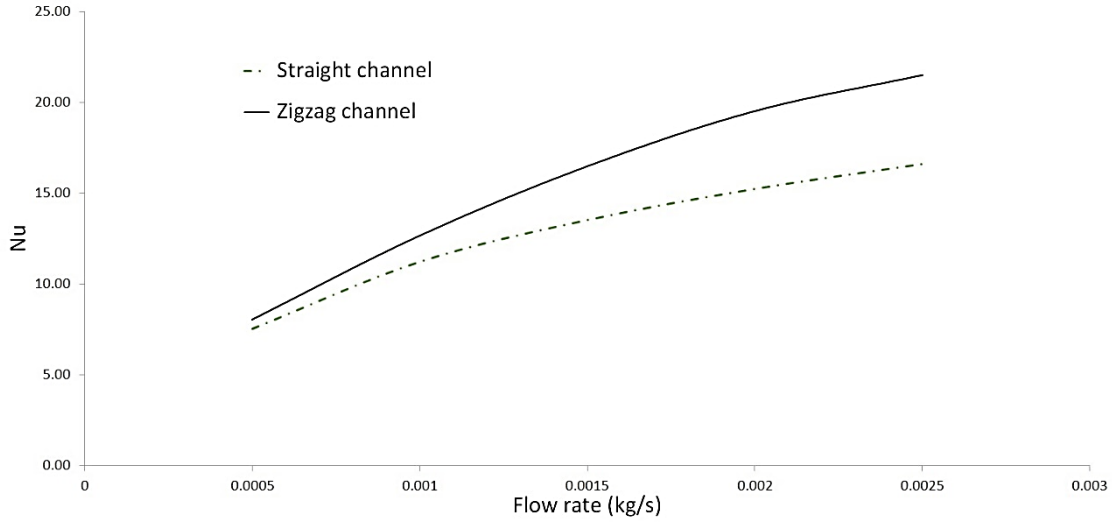

Figure 24 - Variations of nusselt numbers with total flow rate in parallel flow with straight and zigzag channel configuration

Where the higher difference in value is **22.79%** at a flow rate of 0.0025 kg/s.

So, as it can be observed, the **zigzag channel configuration surely offers a better thermal-performance at** the same flow rates, although it comes with a cost in total pressure drop. To clarify the overall performance for these two different configurations, it will be necessary to show the total pumping power required at the different values of thermal resistance obtained for the two channel configurations, figure 26.

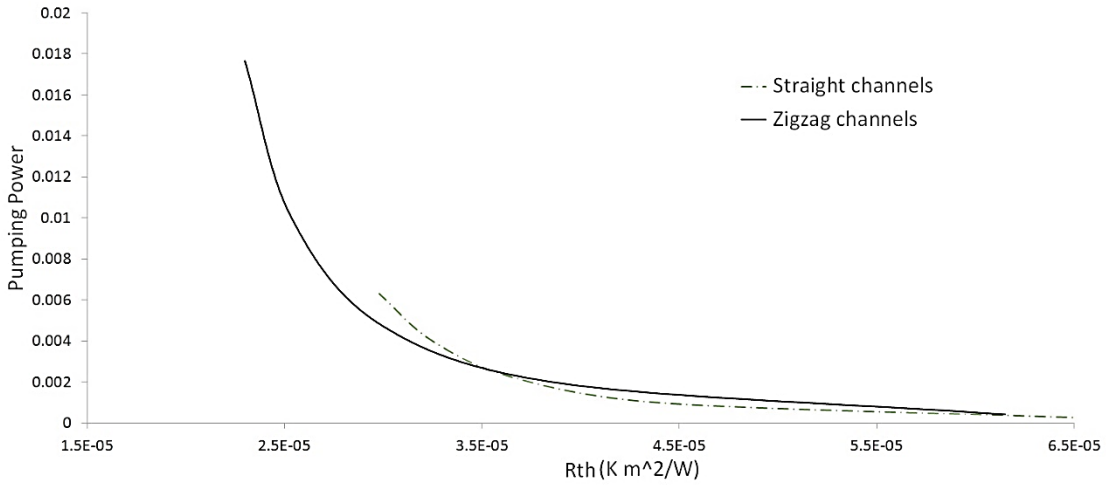

Figure 25 - Thermal resistance related to the pumping power required by the system for straight and zigzag channel configuration in parallel flow

Where interesting results can be observed. For the lower flowrates, the overall performance is slightly better for the straight channel configuration, with very similar results both configurations. Only around flow rates of 0.001 kg/s, is when the zigzag configuration is able to provide lower values of thermal resistance. However, one must be aware of the exponential increment in the total pumping power required for higher flow rates beyond this point. Another important aspect to take into consideration is that only zigzag channel configuration can provide values for thermal resistance under 3 x 10^{-5} $K\,m^2/W$, although with the mention exponential increase in pumping power requirement. **Only for those cases in which a very high cooling requirement applies, and energy supply is not an issue, zigzag configuration would be the desire option** due to the large enhancement to the overall heat sink thermal-performance.

All in all, under the assumptions of this project, any of these two configurations could performed similar results at low flow rates. **Straight channel, though, will be the best option** providing simplicity in geometry for a similar thermal-performance.

According to this project requirements and needs, and the analysis carried on discussing ''counter-parallel'' flow and ''straight-zigzag'' configuration; **parallel flow - straight channel configuration** would be the desire and best option in which to implement the double phase calculations.

4.3. VALIDATION STUDY

Moving forward to final part of this project, using the temperature transforming model, calculations for CASE 1 at different MEPCM particle concentrations were successfully performed in fluent.

A validation study was carried out to ensure the validity and accuracy of the UDF generated and given to ANSYS-FLUENT to solve the energy equation, considering the temperature dependent thermal properties and the source term. The problem solved to do so was the exact analytical solution of the ''one region problem'', without considering natural convection [15]. Different values for the melting temperature range were selected to show the enhancement on the results: temperature distribution along the x direction, and evolution with time of the melting front.

- Geometry

Regarding the phase changing dimensionless analytical resolution of the ''one region problem'', the geometry used was a 2D 1x1 cm simple square geometry. Where the interior is compound by enclosed water surrounded by aluminum walls.

- Boundary conditions

A temperature differential (ΔT). The PCM starting melting temperature on the right side, and a higher temperature of 305 K on the left side. Just comment that any other value of ΔT would be as appropriate as the one selected on the present study. The surrounding walls were adiabatic.

The results for the temperature distribution along x direction at time = 50 seconds, and the melting front location (s) at different times are shown in figure 27. Additionally, the exact values for the variation of the melting front with time, and the error percentage at different ΔT compared to the analytical solution is shown in Table 14.

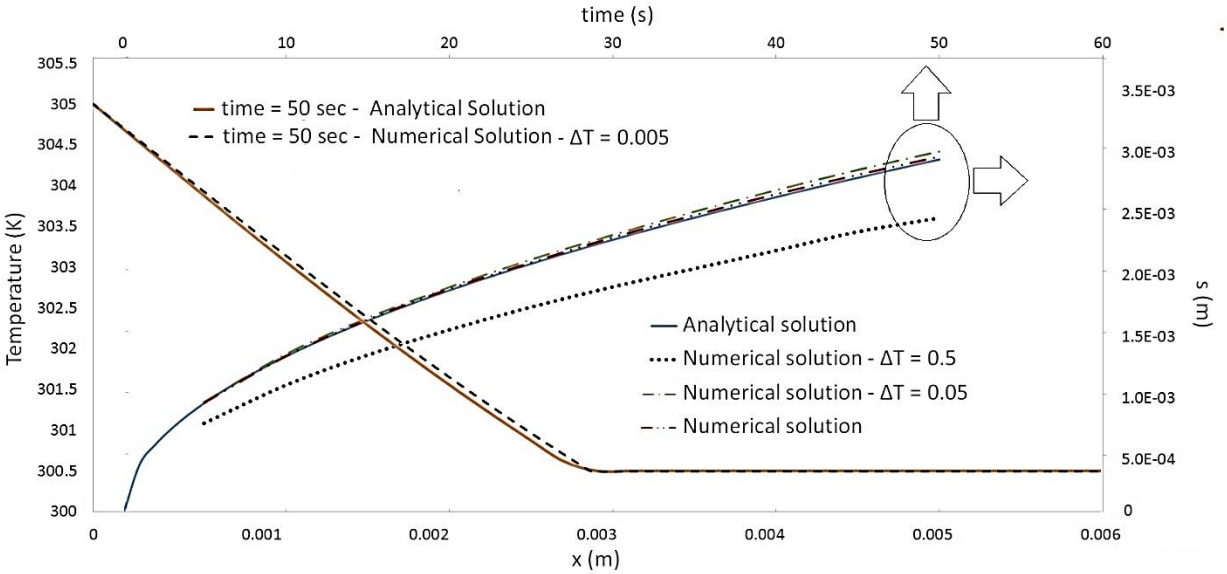

Figure 26 - Temperature distribution at t = 50 sec, and variation of the melting front location with time

Table 14 - Melting front location and error percentage for different ΔT

	Analytic solution	ΔT - 0.5		ΔT - 0.05		ΔT - 0.005	
Time (sec)	s (m)	s (m)	error (%)	s (m)	Error (%)	s (m)	Error (%)
5	0.0009154	0.0007508	**17.98**	0.0009209	**0.604%**	0.0009159	**0.061%**
10	0.0012945	0.0010611	**18.03%**	0.0013113	**1.281%**	0.0012963	**0.138%**
15	0.0015855	0.0013063	**17.61%**	0.0016066	**1.317%**	0.0015917	**0.390%**
20	0.0018307	0.0015115	**17.44%**	0.0018569	**1.408%**	0.0018419	**0.604%**
25	0.0020468	0.0016967	**17.11%**	0.0020821	**1.694%**	0.0020571	**0.499%**
30	0.0022422	0.0018619	**16.96%**	0.0022823	**1.757%**	0.0022613	**0.845%**
35	0.0024218	0.0020100	**17.00%**	0.0024725	**2.0486%**	0.0024425	**0.845%**
40	0.0025890	0.0021572	**16.68%**	0.0026477	**2.2139%**	0.0026126	**0.904%**
45	0.0027461	0.0023100	**15.88%**	0.0028128	**2.3722%**	0.0027708	**0.892%**
50	0.0028946	0.0024224	**16.31%**	0.0029630	**2.3062%**	0.0029183	**0.811%**

As it can be inferred, as the melting temperature range is reduce, the numerical solution gets closer to the analytical one. Lower values of ΔT will lead to an enhancement in accuracy. However, due to the nature of the phase change model and the UDF functions designed, lower values of ΔT will correspond to sharper step functions and bigger differences for the values of specific heat, thermal conductivity and source term at temperatures between $T_m - \Delta T$ and $T_m + \Delta T$. In other words, the lower the temperature melting range is, the more difficulties obtaining full convergence when resolving with fluent that one must deal with.

Regarding to the computational capability available to the author of this project and the intrinsic limitations of the solver, when solving with fluent, accuracy in the results and computational time have been taken to an optimal point. So, even though the temperature transforming model implemented eases the time step, grid size and phase change temperature range selection; the ΔT selected for all calculations has been 1 degrees, which means a total melting range of 2 degrees. Doing so, together with the right time step and relaxation factors selection, led to acceptable values in the convergence.

4.4. DOUBLE PHASE

Finally, the last three cases regarding the addition of MEPCM particles to the current working liquid (water) are going to be presented below. Results for three different micro-particles concentration are discussed in this section, 10, 15 and 20%. Same procedure than used for single phase calculations was followed here. The numerical values obtained for the parameters of interest at the different values of total flow rate are shown in first place; and graphical representation for the overall performance and the behavior of the heat sink along the x direction is added for a better understanding.

For the graphic representations, the three cases here, plus results for case 2 (single phase, straight channel, parallel flow configuration), were plotted together for a better visualization of the enhancement in thermal-performance.

4.4.1. STRAIGHT CHANNELS – Case 2* 10, 15 & 20%

4.4.1.a. Heat Sink performance values

The three cases correspond to the straight channel, parallel flow configuration. The parameters under study for 10, 15 and 20% MEPCM particle concentration, respectively, are shown below in table 15, 16 and 17.

Table 15 - Double phase (PCM concentration 10%) - Straight channels, parallel flow

Total flow rate	**(kg/s)**	**0.0005**	**0.001**	**0.0015**	**0.002**	**0.0025**
Flow rate per channel	(kg/s)	1.52E-05	3.03E-05	4.55E-05	6.06E-05	7.58E-05
v	(m/s)	0.126	0.253	0.379	0.506	0.632
Total Pressure inlet	(Pa)	587.34	1212.08	1865.25	2555.02	3102.57
Total Pressure outlet	(Pa)	10.52	41.32	92.46	163.11	240.68
$T_{s,max}$	(K)	348.99	329.03	324.98	322.52	320.90
u_{avg}	(m/s)	0.126	0.253	0.379	0.506	0.632
P_{ch}	(watt)	8.72E-06	3.55E-05	8.06E-05	1.45E-04	2.17E-04
P_{tot}	(watt)	2.88E-04	1.17E-03	2.66E-03	4.79E-03	7.16E-03
Δp_{ch}	(Pa)	576.82	1170.76	1772.79	2391.92	2861.89
ΔT_{max}	(K)	48.99	29.03	24.98	22.52	20.90
R_{th}	(Km^2/W)	4.90E-05	2.90E-05	2.50E-05	2.25E-05	2.09E-05
$\breve{T}_{max}$		0.089	0.053	0.046	0.041	0.038
$\breve{P}$		3.09E+05	6.27E+05	9.49E+05	1.28E+06	1.53E+06
Nu		10.09	17.03	19.79	21.95	23.66

Table 16 - Double phase (PCM concentration 15%) - Straight channels, parallel flow

Total flow rate	**(kg/s)**	**0.0005**	**0.001**	**0.0015**	**0.002**	**0.0025**
Flow rate per channel	(kg/s)	1.52E-05	3.03E-05	4.55E-05	6.06E-05	7.58E-05
v	(m/s)	0.126	0.253	0.379	0.506	0.632
Total Pressure inlet	(Pa)	705.17	1446.26	2195.66	3026.18	3682.57
Total Pressure outlet	(Pa)	10.46	41.17	92.17	162.06	237.06
$T_{s,max}$	(K)	344.13	328.05	324.05	321.62	319.99
u_{avg}	(m/s)	0.126	0.253	0.379	0.506	0.632
P_{ch}	(watt)	1.05E-05	4.27E-05	9.57E-05	1.74E-04	2.61E-04
P_{tot}	(watt)	3.47E-04	1.41E-03	3.16E-03	5.74E-03	8.62E-03
Δp_{ch}	(Pa)	694.70	1405.08	2103.49	2864.11	3445.51
ΔT_{max}	(K)	44.13	28.05	24.05	21.62	19.99
R_{th}	(Km^2/W)	4.41E-05	2.80E-05	2.40E-05	2.16E-05	2.00E-05
$\breve{T}_{max}$		0.073	0.046	0.040	0.036	0.033
$\breve{P}$		3.14E+05	6.34E+05	9.49E+05	1.29E+06	1.56E+06
Nu		11.20	17.63	20.56	22.86	24.73

Table 17 - Double phase (PCM concentration 20%) - Straight channels, parallel flow

Total flow rate	**(kg/s)**	**0.0005**	**0.001**	**0.0015**	**0.002**	**0.0025**
Flow rate per channel	(kg/s)	1.52E-05	3.03E-05	4.55E-05	6.06E-05	7.58E-05
v	(m/s)	0.126	0.253	0.379	0.506	0.632
Total Pressure inlet	(Pa)	867.14	1788.82	2710.25	3710.78	4480.36
Total Pressure outlet	(Pa)	10.56	41.13	91.96	164.19	235.48
$T_{s,max}$	(K)	338.01	326.25	321.55	319.17	317.85
u_{avg}	(m/s)	0.126	0.250	0.379	0.506	0.632
P_{ch}	(watt)	1.30E-05	5.25E-05	1.19E-04	2.15E-04	3.22E-04
P_{tot}	(watt)	4.27E-04	1.73E-03	3.93E-03	7.11E-03	1.06E-02
Δp_{ch}	(Pa)	856.58	1747.69	2618.30	3546.58	4244.88
ΔT_{max}	(K)	38.01	26.25	21.55	19.17	17.85
R_{th}	(Km^2/W)	3.80E-05	2.62E-05	2.15E-05	1.92E-05	1.79E-05
$\breve{T}_{max}$		0.062	0.043	0.035	0.031	0.029
$\breve{P}$		3.19E+05	6.51E+05	9.76E+05	1.32E+06	1.58E+06
Nu		13.00	18.83	22.94	25.79	27.69

4.4.1.b. Overall thermal-performance

To compare the behavior at different MEPCM particle concentration with the variation on the total flow rate, the next graphs concerning the total pressure drop along the channels, the maximum dimensionless temperature reached at the bottom surface, and nusselt number are presented below in figure 28.

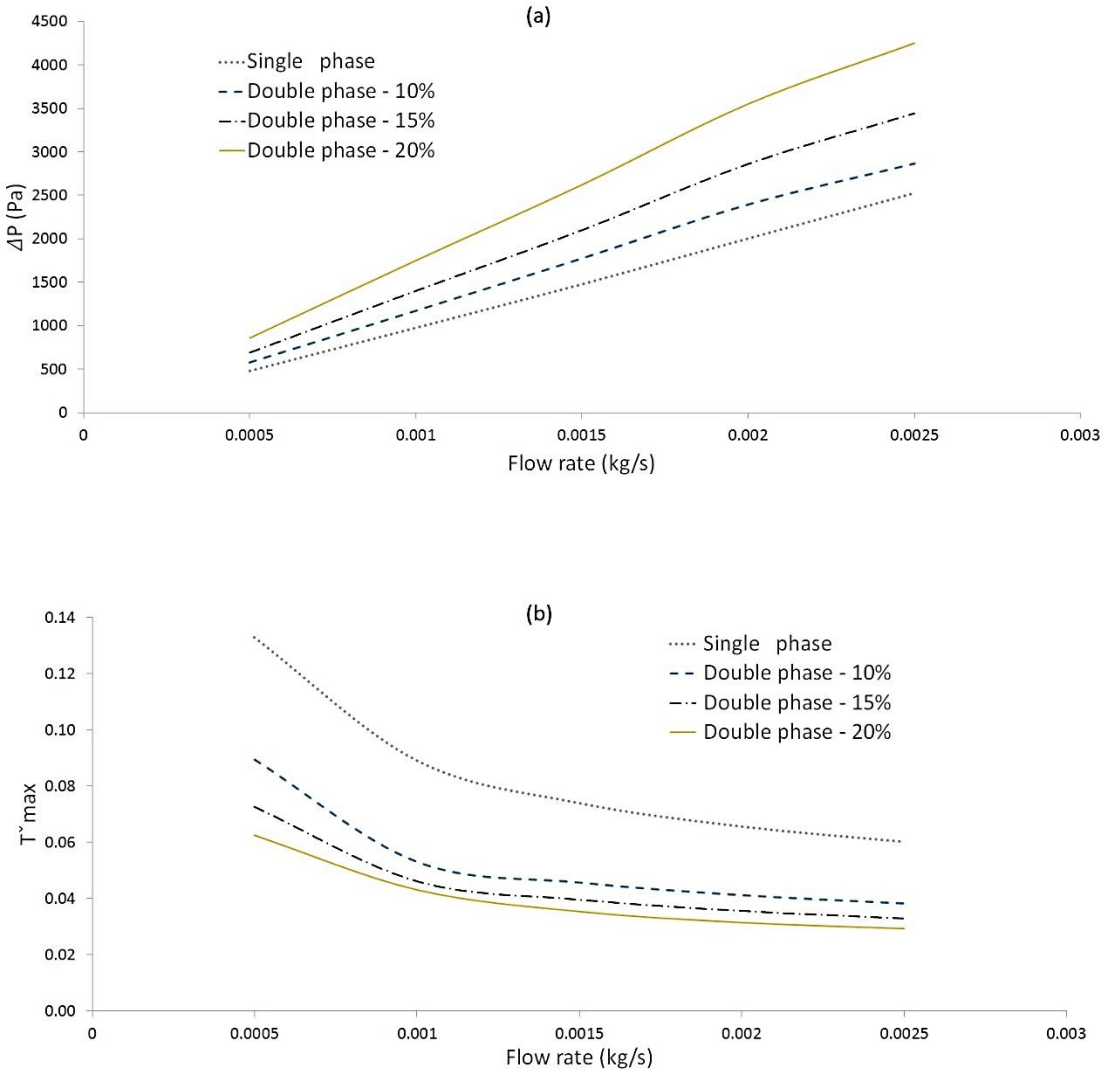

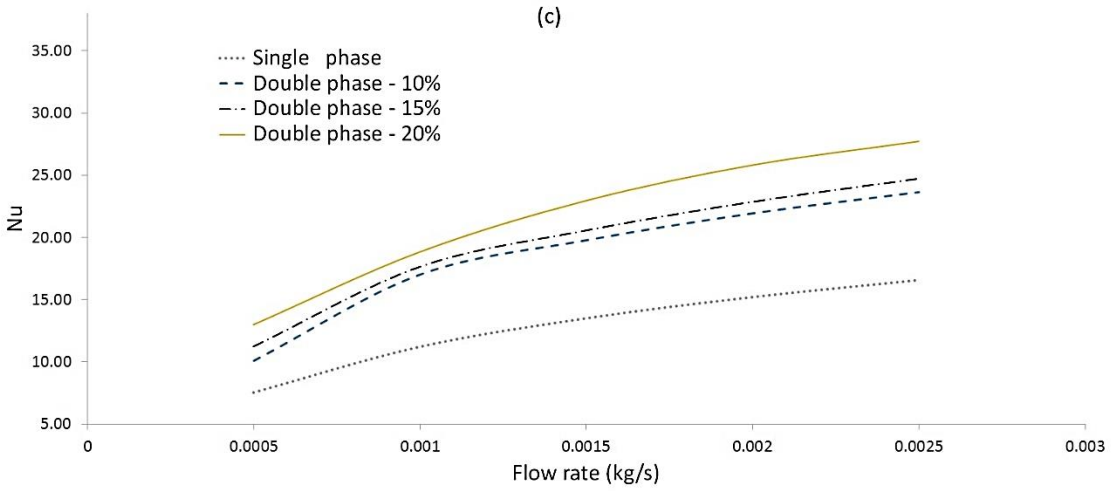

Figure 27 - Variations of (a) total pressure drop, (b) max. dimensionless temperature, and (c) nusselt number with total flow rate in parallel flow with straight channel configuration at different MEPCM particle concentration

Where expected tendencies with the increase in particle´s concentration, for both, pressure and temperature, can be observed. As the effective viscosity of the slurry increases, higher values of total pressure drop, for the same total flow rate values, are obtained. Also, as a remarkable fact, the slope of these tendency lines plotted at different MEPCM concentration, in figure 28.a, and regarding the pressure drop increment with the total flow rate, is larger at higher particle´s concentrations. This fact should be taken into consideration when adding the melting material because the enhancement in temperature could not be enough to compensate the extra pumping power required to the system.

On the other hand, as a positive aspect, **the global thermal behavior is significantly improved at all flow rates**. In this case, the dimensionless temperature and the nusselt number were chosen to show the thermal-performance enhancement. Both representations keep similar tendencies with the variation in particle´s concentration and total flow rate. The reduction in maximum temperature at the bottom surface exhibited is different as we change the heat sink´s operation point. In this study, an optimal operational point is being searched, so it was necessary to measure this different enhancement differences to find the better working condition for the greater thermal improvement. The differences in percentage for the maximum temperature reached at the bottom surface, at the different MEPCM particle concentration and for the lower and higher flow rates are shown in Table 18.

Table 18 -Differences in percentage in maximum temperature reached at the bottom surface between single phase and double phase calculations at different flow rates and MEPCM particle concentration

		MEPCM concentration (%)		
		10	**15**	**20**
Flow rate (kg/s)	**0.0005**	4.57	5.90	7.57
	0.0015	3.45	3.73	4.47
	0.002	2.70	2.97	3.62

Where the bigger differences, obviously, were observed for 20% MEPCM particle concentration. All in all, **the higher relative overall thermal enhancement is given at lower flow rates**. Indeed, from

figure 28.b, c one can inferred that **the bigger differences in maximum temperature, and so in thermal improvement, are located around a total flow rate value 0.001 kg/s and below.**

Additionally, the next global performance parameters: thermal resistance per total pumping power required, and thermal resistance and dimensionless total pressure drop with the variation in total flow rate, are introduced in figure 29.

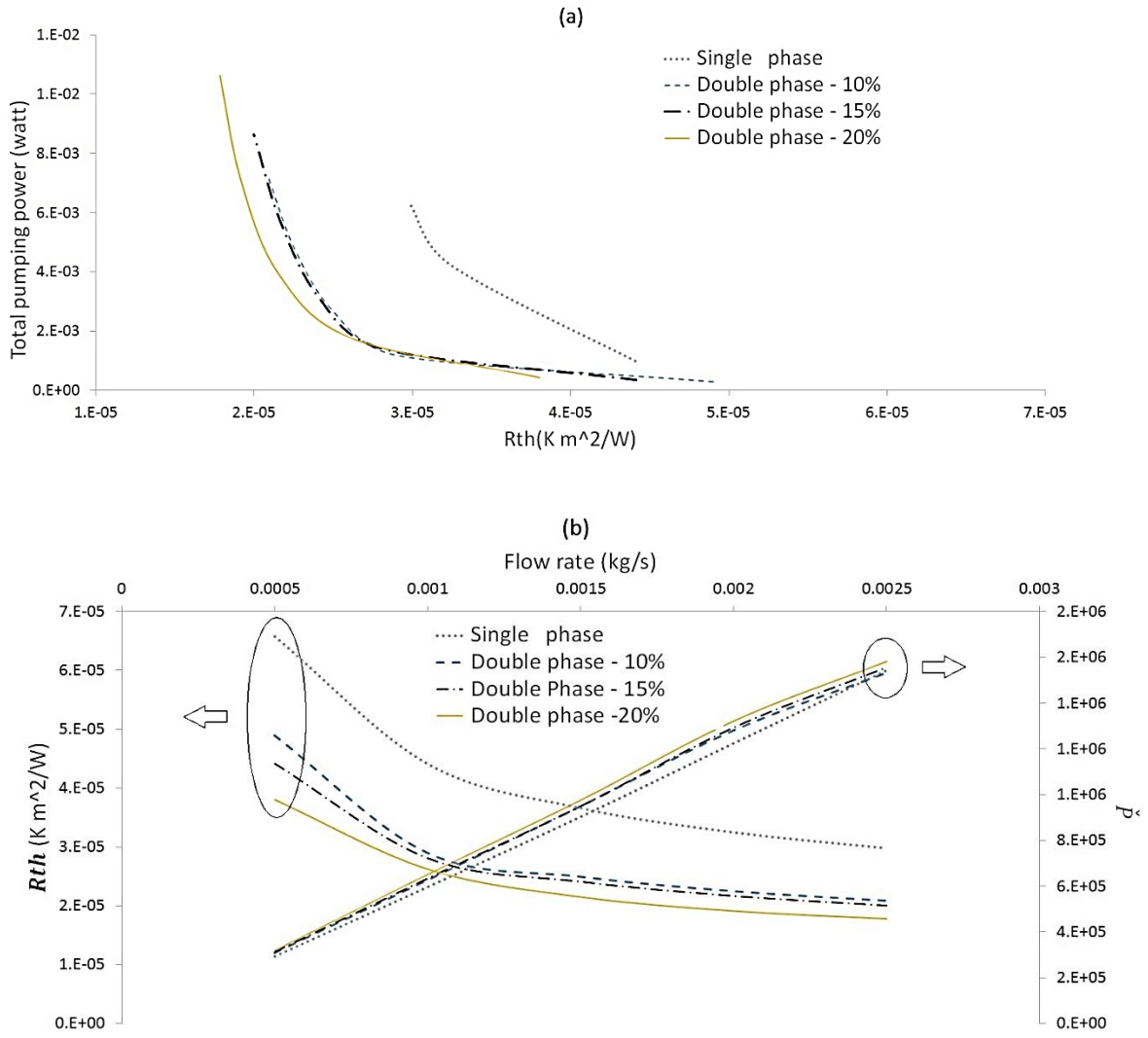

Figure 28 - Variations of (a) total pumping power, and (b) dimensionless pressure drop and thermal resistance with total flow rate in parallel flow with straight channel configuration at different MEPCM particle concentration

Where similar conclusions could be extracted from the thermal resistance plotted in figure 29.b. The dimensionless total pressure drop, on the other hand, shows an interesting characteristic. Basically, the same almost linear relation with the flow rate concerning the increment in pressure drop is obtained regardless the MEPCM concentration.

To conclude the overall thermal-performance, referring to figure 29.a, several aspects are observed.

Firstly, **MEPCM particle addition means positive thermal-performance enhancement always**, allowing to the heat sink device to cool down the heat source surface under single phase reached values; and so, reaching thermal resistance to pumping power values that single phase is not capable of giving. Also, the **slurry thermal-properties offer a better relation between minimum thermal resistance value performed and pumping power required until thermal resistance values around 2.8 x 10^{-5}**; where a notable cooling improvement is made at a lower energy cost. Under this limit, increasing the MEPCM particle concentration will lead to even lower thermal resistance values, but at an exponential increment in pumping power cost.

At the same time, **with regard to thermal resistance to pumping power values at low flow rates, one can conclude that the three different slurries at different particle´s concentration offer similar overall thermal-performance.** Particularly, slurries at 10 and 15% particle´s concentration exhibit a very similar thermal behavior among the total flow rates studied. Only over 20% in particle´s concentration, the heat sink will be able to get to lower thermal resistance values.

4.4.1.c. Heat sink behavior throughout the channels

After discussing the overall performance, the slurry behavior at different MEPCM particle concentration throughout the fluid channel and bottom surface regarding the mean temperature distribution throughout the fluid channel and bottom surface is shown below. Figure 30.

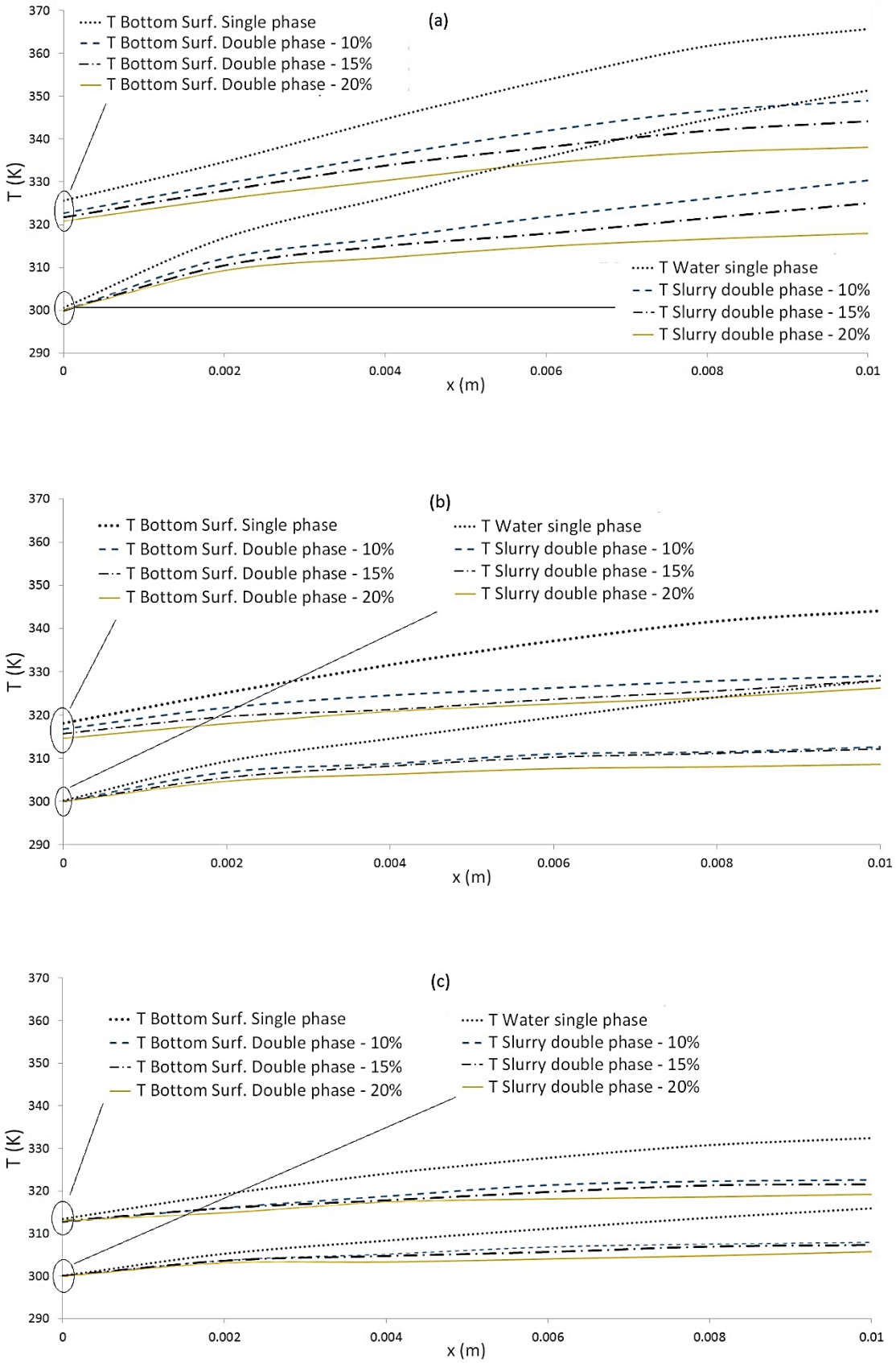

Figure 29 - Mean temperature distribution throughout the fluid channel and the bottom surface at (a) 0.0005, (b) 0.001 and (c) 0.002 kg/s for parallel flow with straight channel configuration at different MEPCM concentrations

Where, as the main characteristic observed, **the addition of MEPCM particles provides to both, fluid and solid bottom heated surface a bigger homogeneity in temperature along the longitudinal direction;** being greater the level of homogeneity at higher MEPCM particle concentrations**.** Differences between slurries diminish with the increment in total flow rate. This fact means a very important finding, because the addition of melting micro-particles to a single phase cooling liquid, with parallel flow, gives to the device the advantages offered by the counter flow configuration, keeping a better level of homogeneity at the bottom surface. Besides, as discussed in the previous single phase results section, parallel flow gets to keep a lower temperature along almost the whole channels. Therefore, **considering the lower temperature values given by the parallel flow configuration in comparison with counter flow for most of the heat sink body; together with the increment in homogeneity that the addition of MEPCM particles can provide, an optimal heat sink configuration can be obtained.** Where, although a counter flow configuration would provide a higher level of homogeneity due to the nature of its design, with a parallel flow configuration an overall lower thermal distribution could be obtained at a very similar temperature homogeneity level.

To illustrate the previous graphs in figure 30, contour plots for pressure and temperature distribution were added. Contours for the three different slurries at different particle´s concentrations are shown together for a better comparison.

- Bottom surface temperature distribution:

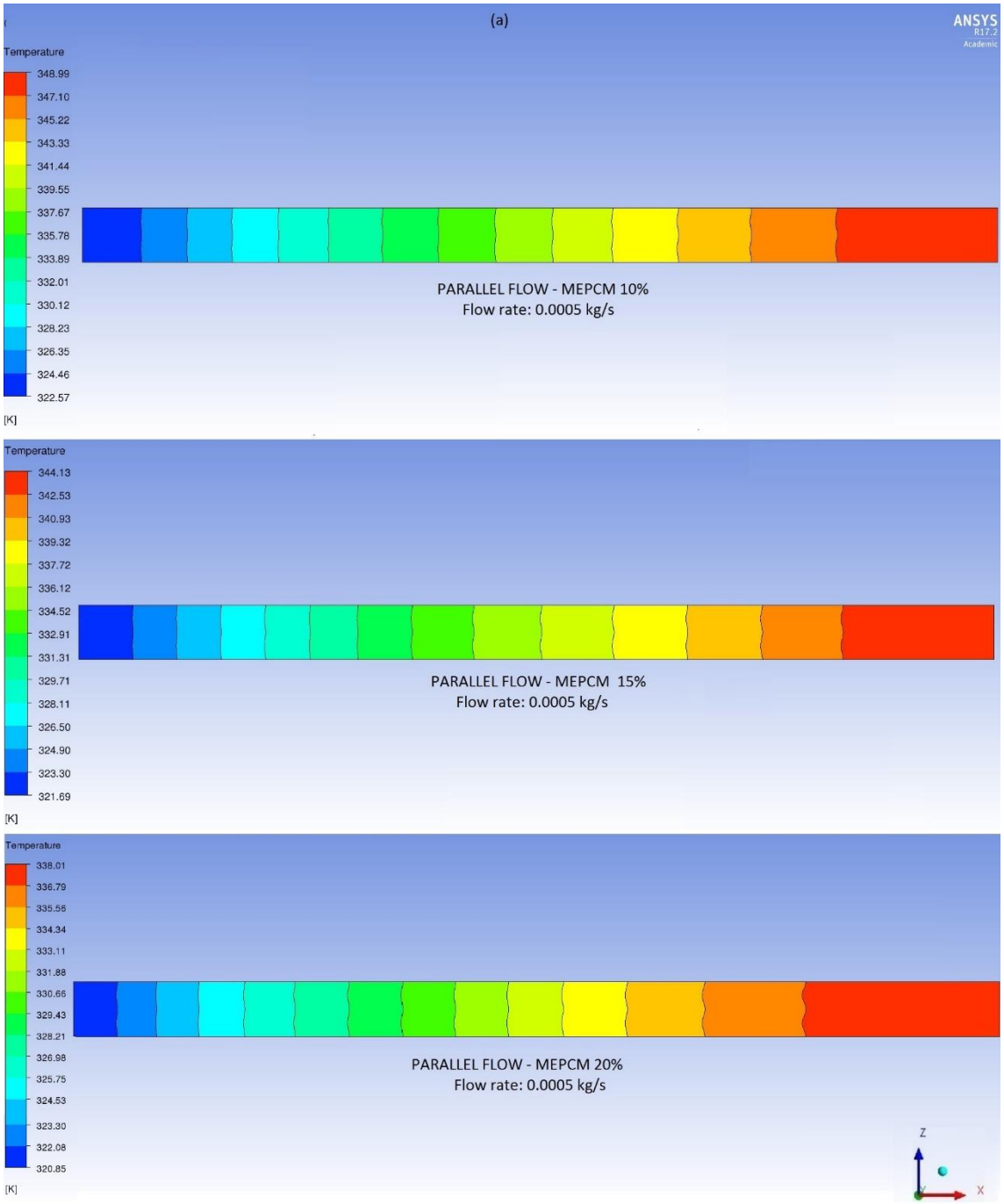

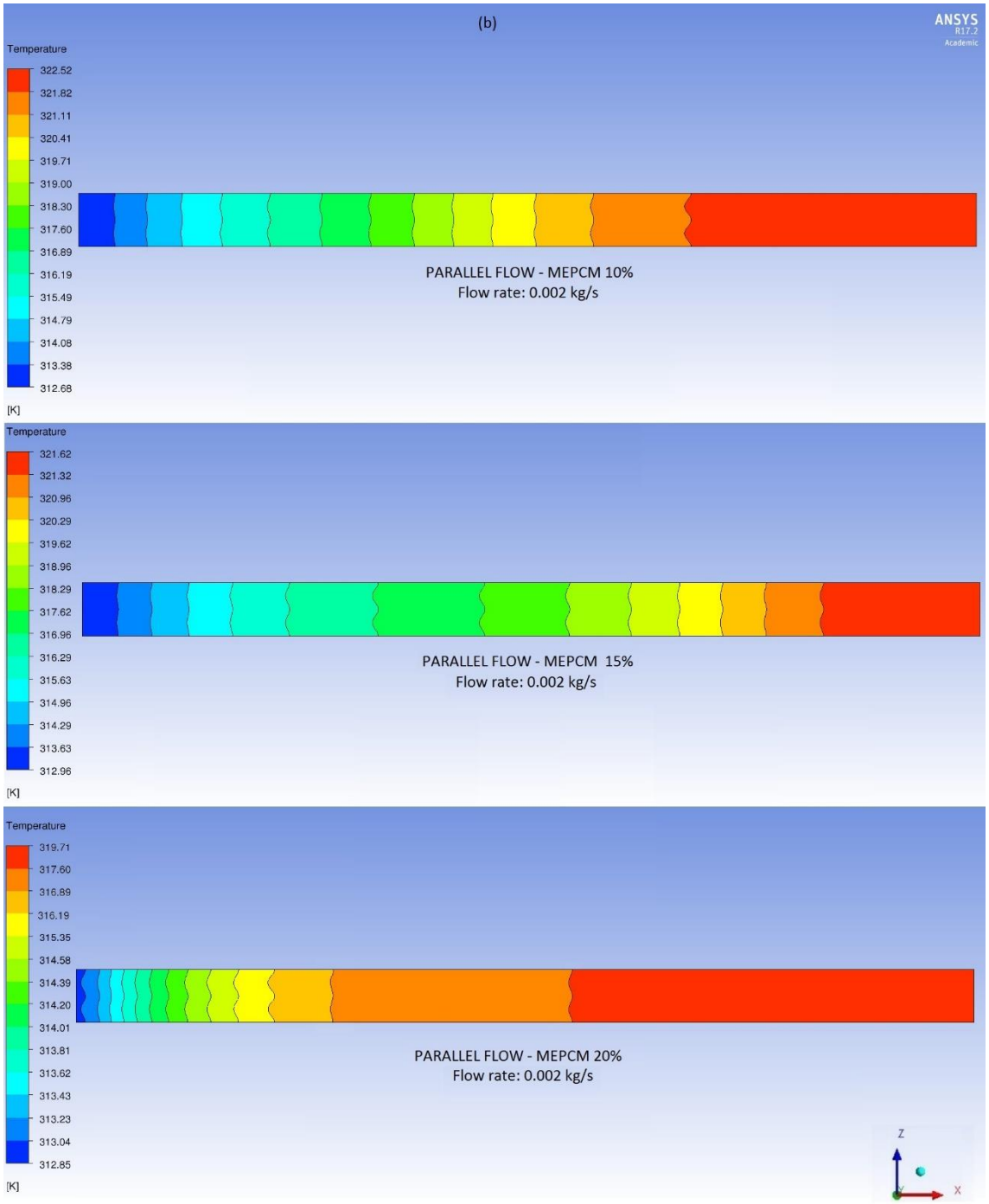

Figure 30 – Temperature contours at the bottom surface at (a) 0.0005 and (b) 0.002 kg/s in parallel flow with straight channel configuration at different MEPCM concentrations

- Vertical symmetry plane temperature distribution:

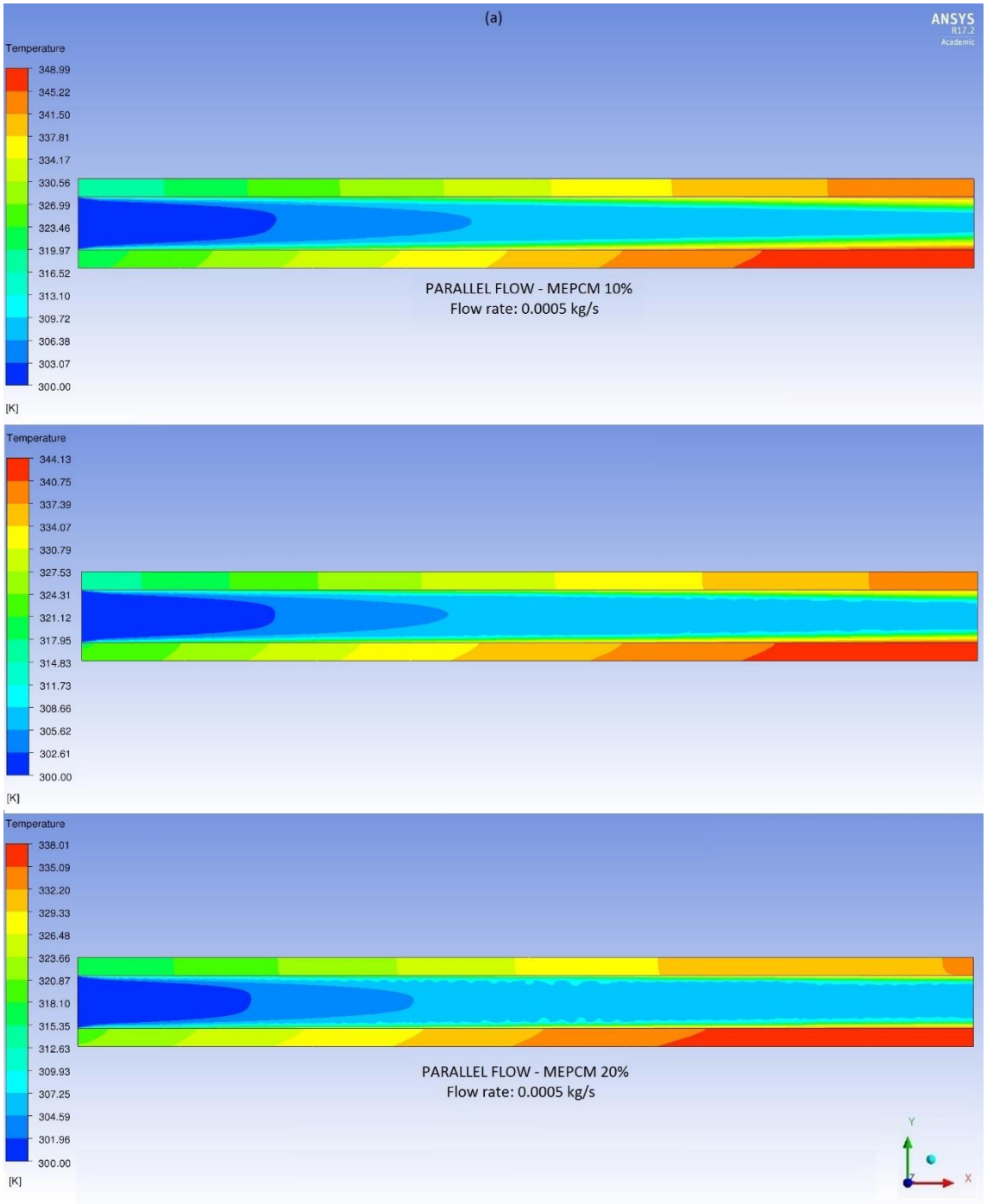

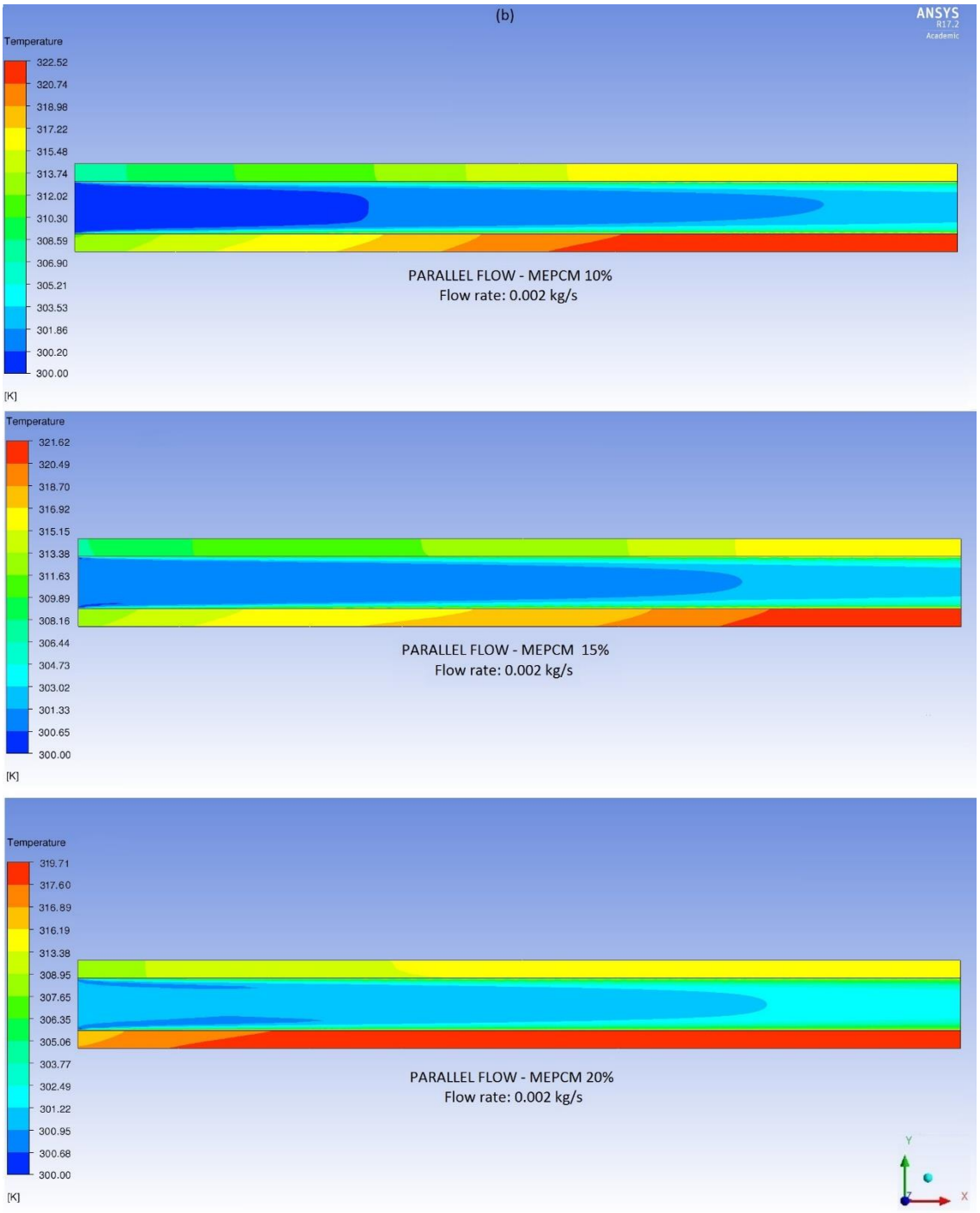

Figure 31 – Temperature contours throughout the vertical symmetry plane at (a) 0.0005 and (b) 0.002 kg/s in parallel flow with straight channel configuration at different MEPCM concentrations

Regarding figures 31 and 32, as the MEPCM particle concentration and the total flow rate are increased, a greater temperature homogeneity is achieved. The higher the flow rate and particle´s concentration, the clearer that these results can be observed. Comparing these two figures with figures 10 and 11 from single phase results, one can easily conclude the improvement in the heat sink thermal working conditions.

- Vertical symmetry plane total pressure distribution:

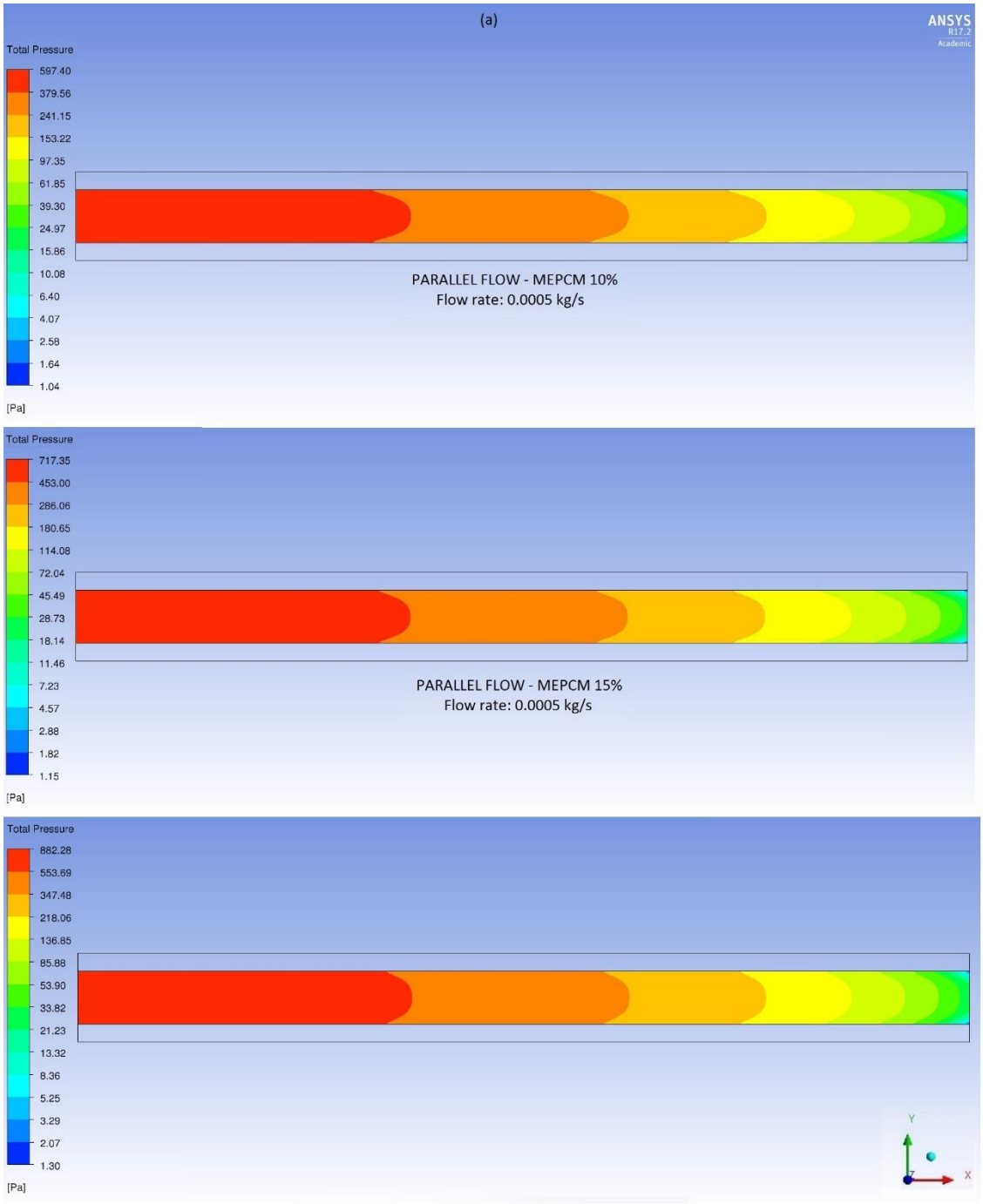

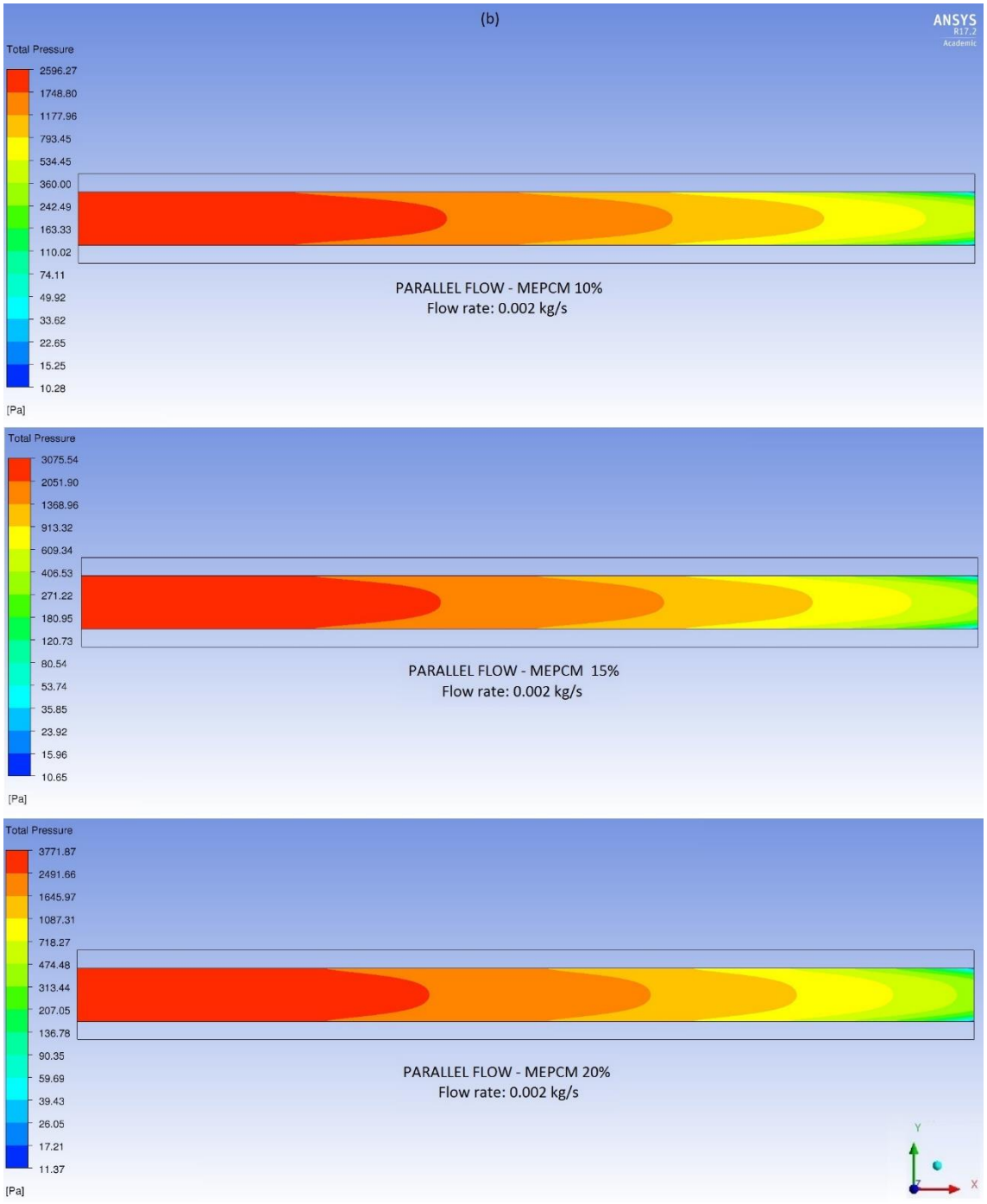

Figure 32 – Total pressure contours throughout the vertical symmetry plane at (a) 0.0005 and (b) 0.002 kg/s in parallel flow with straight channel configuration at different MEPCM concentrations

Where the total pressure distribution has been chosen in this case to, somehow, show the similarities in the static pressure distribution at different MEPCM particle concentration at the same flow rate; but also, to illustrate the small discrepancies in the dynamic pressure due to the increase in viscosity. Which can be observed in the contour profiles from the different pressure value levels.

Additionally, as the main added characteristic to double phase calculations, it will be necessary to show the specific heat capacity values for the slurry throughout the channels. This parameter, as defined as a step function within the melting temperature range, will determine, in an approximate way, the melting front location; where those MEPCM particles involved in the melting process, at a certain time, will have the highest values of specific heat.

In figures 34 to 36 specific heat capacity contour plots are shown at different flow rates for 10% slurry MEPCM particle concentration.

- Vertical symmetry plane specific heat distribution:

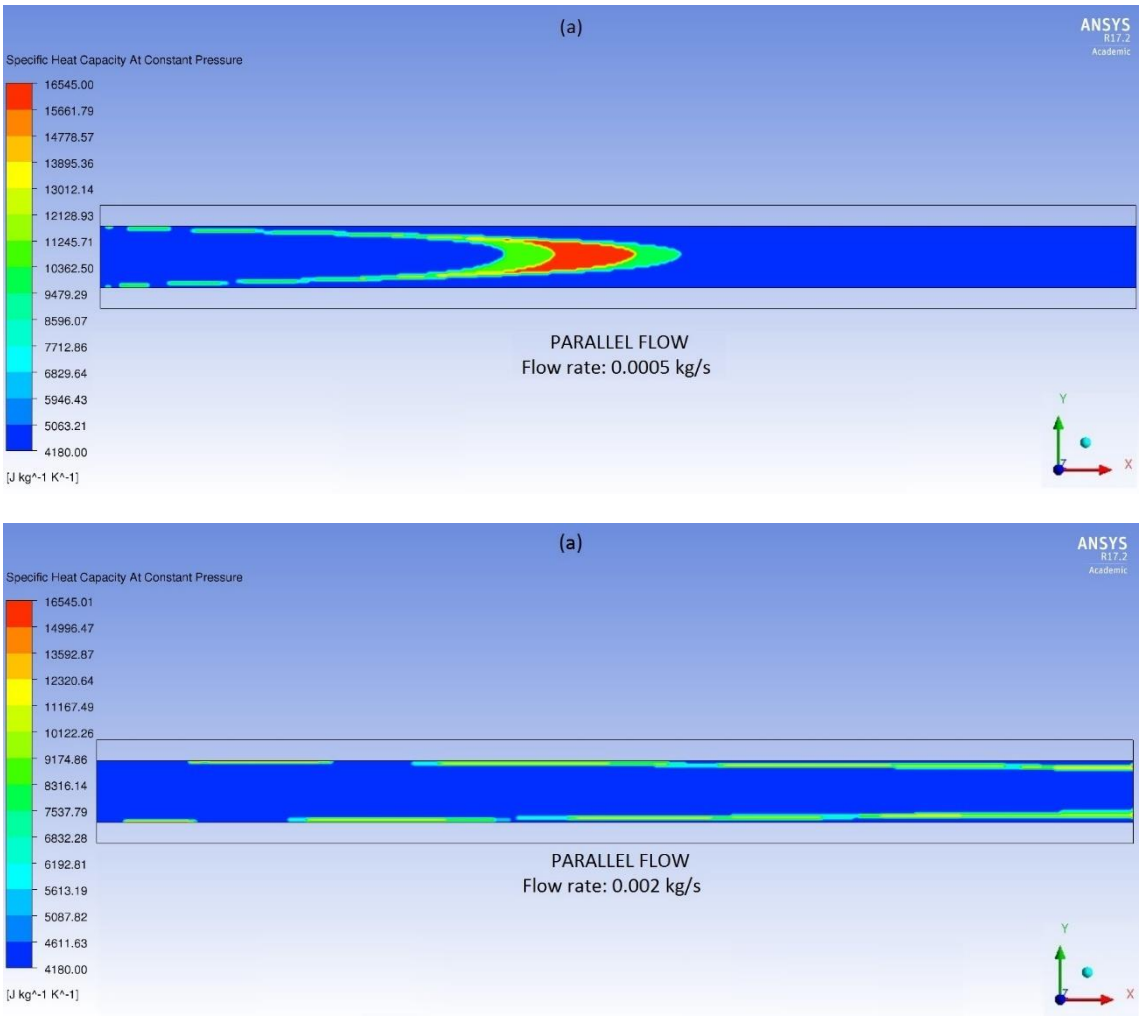

Figure 33 – Specific heat contours throughout the vertical symmetry plane at (a) 0.0005 and (b) 0.002 kg/s in parallel flow with straight channel configuration at 10% MEPCM concentration

- Fluid volume specific heat capacity distribution:

Additionally, to better represent the melting process occurring within the channels, the specific heat contours for the whole fluid volume along the micro-channel are shown below:

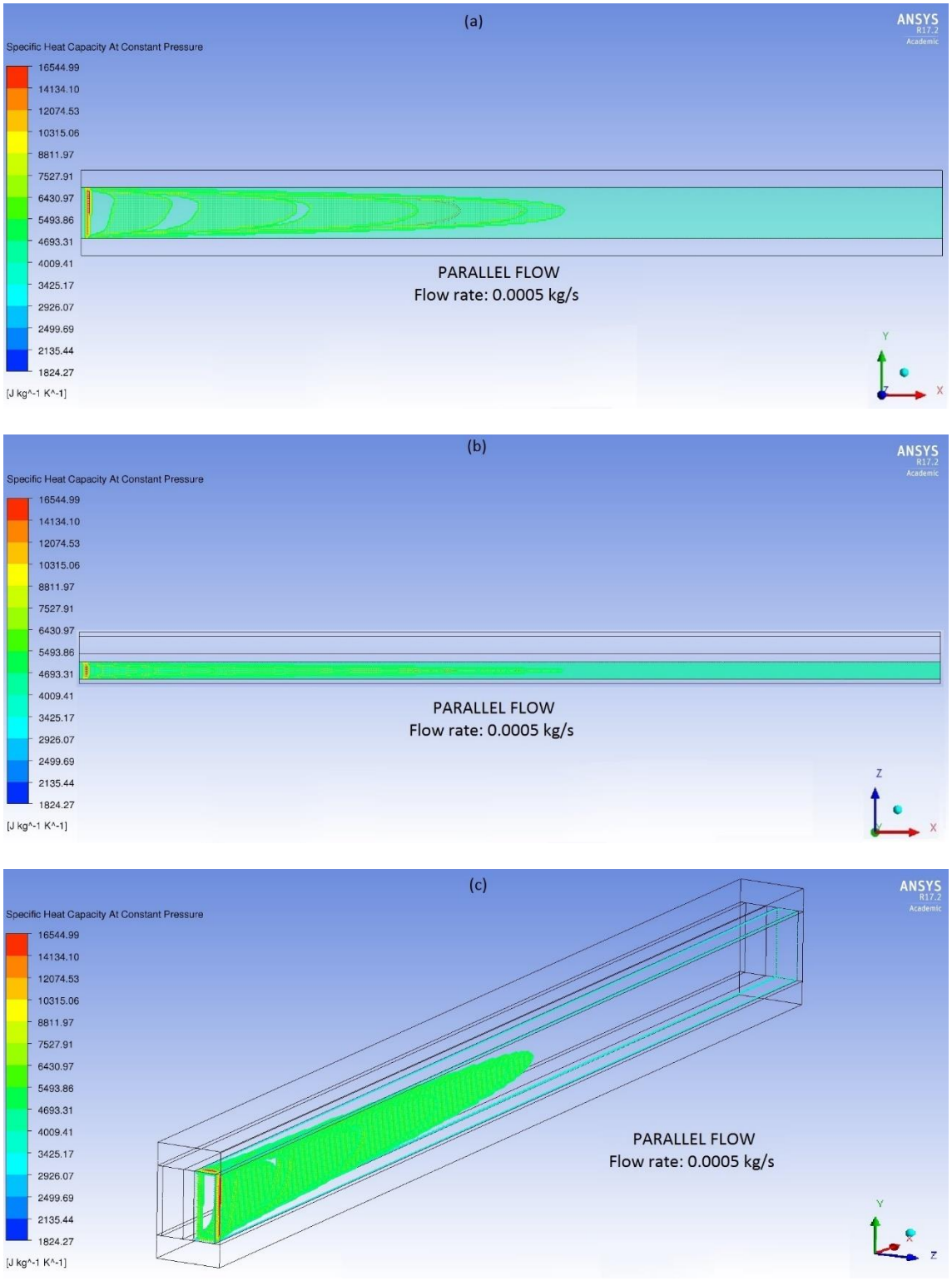

Figure 34 - Specific heat contours within the fluid channel seen from (a) side, (b) up and (c) 3D perspective at 0.0005 kg/s in parallel flow with straight channel configuration at 10% MEPCM concentration

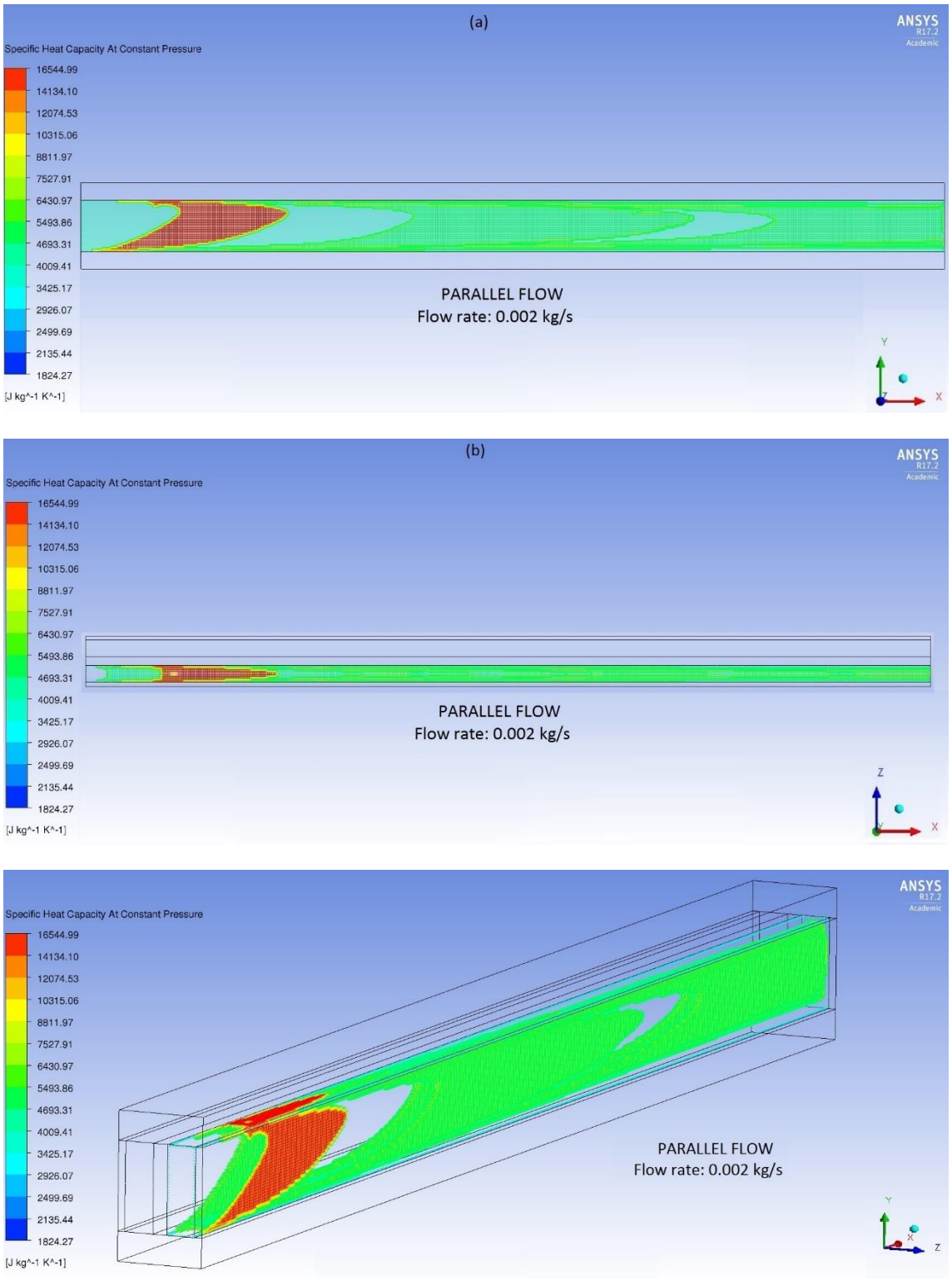

Figure 35 - Specific heat contours within the fluid channel seen from (a) side, (b) up and (c) 3D perspective at 0.002 kg/s in parallel flow with straight channel configuration at 10% MEPCM concentration

As shown in the previous contour plots, **the flow rate will define the particle melting distribution**, which has an important influence in the temperature distribution along the channels. In particular, as *R. Sabbah, Mohammad M.Farid, S. Al-Hallaj* [8] proved, to get remarkable enhancement for a certain heat flux, the cooling system should be designed so that the MEPCM particles start melting

at the channel inlet and they should be completely melted by the time the particles reach the channel exit. Doing so, a higher temperature homogeneity for the cooling fluid can be reached.

This same fact has been shown in figure 30, together with figures 34 to 36; where temperature throughout the channels was kept at a lower and more constant value as the total flow rate increases. And the reason why is because of the particle melting distribution. Comparing these two flow rates, 0.0005 and 0.002 kg/s, only for the higher value the *R. Sabbah, M.Farid* and *Al-Hallaj* is satisfied.

5. CONCLUSIONS

A three-dimensional numerical study was developed to analyze the heat transfer enhancement of a micro-channel heat sink. Single and double phase, counter and parallel flow, together with straight and zigzag channel geometry configuration, and a better modelling approximation for the melting/solidification process have been the characteristics examined regarding the heat sink performance. The effect of the flume and channel geometry configuration at different coolant flow rates on the temperature distribution of the heat sink have been investigated. The main findings are listed below:

Regarding parallel and counter flow configuration, and considering the minimum value of thermal resistance performed by the heat sink, counter flow configuration offers a slightly overall better cooling performance, with a better homogeneity in temperature at the bottom surface. However parallel flow provides better results cooling down the heat sink to lower values than the counter flow configuration does for the most part of the heat sink body. Parallel flow provides a better thermal-performance along the heat sink micro-channels.

Comparing straight and zig zag geometry channel configuration, zigzag channels offer a better thermal-performance, cooling down the heated surface to lower values than the straight channels, although it comes with a cost in the total pressure drop. However, considering the relation between thermal resistance and total pumping power required, the discrepancies between thermal-performances between these two channel configurations fade away. At the lower flowrates, the overall performance is slightly better for the straight channel configuration, with very similar results for both configurations. Only when lower values of thermal resistance are asked to the system; zigzag channel configuration is the only option that can provide those. However, one must be aware of the exponential increment in the total pumping power required at higher flow rates. Only for those cases in which a very high cooling requirement applies, and energy supply is not an issue, zigzag configuration would be the desire option. All in all, at low flow rates the straight channel configuration offers a pretty good thermal-performance with a minimum drop in the total pressure.

To conclude**, referring to the double phase calculations, where MEPCM particles at different concentrations were added to water,** the results obtained showed a notable enhancement in the thermal-performance of the heat sink at all flow rates. Parallel flow, straight channel configuration was picked as the case to which apply the multi-phase melting characteristics. Increasing mass concentration led to better thermal-performance, although this improvement come with an increase in pressure drop. Also, the bigger differences in temperature are located around a total flow rate of 0.001 kg/s and below, so therefore, the relative higher overall thermal enhancement is given at lower flow rates.

Regarding the relation between thermal resistance and total pumping power required, MEPCM particle addition means positive thermal-performance enhancement always, reaching thermal resistance to pumping power values that single phase is not able to give. Also, at low flow rates, MEPCM particle addition offers a better ratio between thermal-performance enhancement and pumping power compare to single phase cooling liquids. Which means better thermal-performance

at a lower energy cost. Increasing the total flow rate over 0.001-0.0015 kg/s will lead to even lower thermal resistance values, but at an exponential increment in pumping power cost. Also, as a significant fact, around values of 2.8 x 10^{-5} Km^2/W and above for thermal resistance, the three different slurries at different particle´s concentration offer similar overall thermal-performance

Finally, emphasize that the addition of MEPCM particles provides to both, fluid and solid bottom heated surface a better homogeneity in temperature along the longitudinal direction. What is more, the flow rate will define the particle melting distribution throughout the channels, getting better temperature homogeneity performances for higher values of total flow rate.

6. REFERENCES

1. F. J. Hong, P. Cheng, H. Ge, and Goh Teck Joo, Conjugate Heat Transfer in Tree-shape Micro-Channel Network Heat Sink for Integrated Microelectronic Cooling Application, Int. J. Heat Mass Transfer, vol. 25, pp. 986–998, 2007.

2. D. B. Tuckerman and R. F. W. Pease, High-Performance Heat Sinking for VLSI, Electron Device Lett., IEEE, vol. 2, pp. 126–129, 1981.

3. W. Qu and I. Mudawar, Experimental and Numerical Study of Pressure Drop and Heat Transfer in a Single Phase Micro-Channel Heat Sink, Int. J. Heat Mass Transfer, vol. 45, pp. 2549–2565, 2002.

4. Afzal Husain, Kwang-Yong Kim, Optimization of a micro-channel heat sink with temperature dependent fluid properties, Applied Thermal Engineering vol. 28, pp. 1101–1107, 2008.

5. K. Vafai, L. Zhu, Analysis of two layered micro channel heat sink concept in electronic cooling, International Journal of Heat and Mass Transfer vol. 42, pp. 2287-2297, 1999.

6. D. Ansari, Kwang-Yong Kim, Double-Layer Micro-Channel Heat Sinks with Transverse- Flow Configurations, Journal of Electronic Packaging, vol. 138 / 031005-1, 2016.

7. F. Zhang, B. Sunden, W. Zhang, G. Xie, Constructal parallel-flow and counter-flow micro-channel heat sink with bifurcations, Numerical Heat Transfer, Part A, 68: 1087–1105, 2015.

8. R. Sabbah, Mohammad M.Farid, S. Al-Hallaj, Micro-channel heat sink with slurry of water with micro-encapsulated phase change material: 3D-numerical study, Applied Thermal Engineering vol. 29, pp. 445-454, 2008.

9. S. Kuravi, Krishna M. Kota, J. Du and Louis C. Chow, Numerical investigation of flow and heat transfer performance of nano-encapsulated phase change material slurry in micro-channels, Journal of heat transfer vol. 131, 062901-1, 2009.

10. B. Rajabifar, Hamid R. Seyf, Y. Zhang, Sanjeev K. Khanna, Flow and heat transfer in micro pin fin heat sinks with nano-encapsulated phase change materials, Journal of heat transfer vol. 138/062401-1, 2016.

11. Goel, M., Roy, S. K., and Sengupta, S., 1994, Laminar Forced Convection Heat Transfer in Microencapsulated Phase Change Material Suspension, Int. J. Heat Mass Transfer, 37(4), pp. 593–604.

12. Inaba, H., 2004, Melting Heat Transfer Characteristics of Microencapsulated Phase Change Material Slurries with Plural Microcapsules Having Different Diameters, ASME J. Heat Transfer, 126, pp. 558–565.

13. S. Petrescu, Comments on the optimal spacing of parallel plates cooled by forced convection, Int. J. Heat Mass Transfer 37 (1994) 1283.

14. S. Bhattacharjee, W.L. Grosshandler, The formation of wall jet near a high temperature wall under microgravity environment, ASME HTD 96 (1988) 711- 716.

15. Amir Faghri, Yuwen Zhang,Transport Phenomena in Multiphase Systems, 2006, Elsevier.

16. ANSYS FLUENT User´s Guide.

17. S. K. Roy and S. Sengupta, An evaluation of phase change microcapsules for use in enhanced heat transfer fluids, Int. Commun. Heat Mass Transfer 18, 495.-507 (1991).

18. M. Gael. Laminar forced convection heat transfer in microencapsulated phase change material suspensions. M.S.M.E. Thesis, University of Miami, FL (1992).

19. E. C. Guyer and D. L. Brownell, Handbook of Applwd Thwmui Design. McGraw-Hill, New York (1988).

20. V. Vand, Theory of viscosity of concentrated suspensions, Nature 155, 364365 (1945).

21. J. C. Maxwell, A Treutisc on Electr~iry und Mcqctism. Vol. I. pp. 440441. Dover. New York (1954).

22. E. Yamada and K. Takahashi, Effective thermal conductivity of suspensions-1st Report, **Heni** Trcmsftir Jup. Res. 4, 83-101 (1975).

23. S. Kuravi, K.M. Kota, J. Du, L. Chow, Numerical investigation of flow and heat transfer performance of nano-encapsulated phase change material slurry in micro-channels, J. Heat Transfer 131 (2009) 0629011–0629019.